

UNIVERSITY OF WARMIA AND MAZURY IN OLSZTYN

Technical Sciences

16(2)



PUBLISHER UWM

Editorial Board

Ceslovas Aksamitauskas (Vilnius Gediminas Technical University, Lithuania), Stefan Cenkowski (University of Manitoba, Canada), Adam Chrzanowski (University of New Brunswick, Canada), Davide Ciucci (University of Milan-Bicocca, Italy), German Efremov (Moscow Open State University, Russia), Mariusz Figurski (Military University of Technology, Poland), Dorota Grejner-Brzezinska (The Ohio State University, USA), Janusz Laskowski (University of Life Sciences in Lublin, Poland), Lech Tadeusz Polkowski (Polish-Japanese Institute of Information Technology, Poland), Vladimir Tilipalov (Kaliningrad State Technical University, Russia), Alojzy Wasilewski (Koszalin University of Technology, Poland)

Editorial Committee

Marek Markowski (Editor-in-Chief), Piotr Artiemjew, Kamil Kowalczyk, Wojciech Sobieski, Piotr Srokosz, Magdalena Zielińska (Assistant Editor), Marcin Zieliński

Features Editors

Piotr Artiemjew (Information Technology), Marcin Dębowski (Environmental Engineering), Marek Mróz (Geodesy and Cartography), Ryszard Myhan (Biosystems Engineering), Wojciech Sobieski (Mechanical Engineering), Piotr Srokosz (Civil Engineering), Jędrzej Trajer (Production Engineering)

Statistical Editor

Paweł Drozda

Executive Editor

Mariola Jezierska

The Technical Sciences is indexed and abstracted in BazTech (<http://baztech.icm.edu.pl>) and in IC Journal Master List (<http://journals.indexcopernicus.com>)

The Journal is also available in electronic form on the web sites

<http://www.uwm.edu.pl/techsci> (subpage Issues)

<http://wydawnictwo.uwm.edu.pl> (subpage Czytelnia)

The print edition is the primary version of the Journal

PL ISSN 1505-4675

© Copyright by Wydawnictwo UWM • Olsztyn 2013

Address

ul. Jana Heweliusza 14
10-718 Olsztyn-Kortowo, Poland
tel.: +48 89 523 36 61
fax: +48 89 523 34 38
e-mail: wydawca@uwm.edu.pl

Contents

I. Bauer, A. Baryga – <i>Tribocorrosion of a Chromosiliconized Layer</i>	85
W. Sobieski – <i>The Basic Closures of Fluid Mechanics in form Characteristic for the Finite Volume Method</i>	93
Z. Kaliniewicz – <i>Two Mathematical Formulas for Assessing Seed Separation Efficiency</i>	109
Z. Kaliniewicz – <i>String Sieve: Design Concept and Parameters</i>	119
J. Jaroszewicz, Ł. Dragun – <i>Limitation of Cauchy Function Method in Analysis for Double Estimators of Free Transversal Vibration of Cantilever Tapered Shafts</i>	131
W. Błaszczak-Bąk, A. Sobieraj – <i>Impact of Optimization of Als Point Cloud on Classification</i>	147

TRIBOCORROSION OF A CHROMOSILICONIZED LAYER

Iwona Bauer^{1*}, *Andrzej Baryga*²

¹ Chair of Materials and Machinery Technology
University of Warmia and Mazury in Olsztyn

² Institute of Agricultural and Food Biotechnology
Department of Sugar in Leszno

Received 3 February 2013; Accepted 17 April 2013; Available on line 15 July 2013

Key words: chromosiliconizing, tribocorrosion, sugar slurry.

Abstract

The paper presents the results of an experiment investigating the tribocorrosion of C45 steel samples which were chromosiliconized by the powder-pack method.

The technological process was carried out at 1000°C for 6 hours. The layer was produced with the use of ferrochromium powder combined with SiC, kaolin and ammonium chloride. Analytical samples were placed in boxes containing the powder mix, and the boxes were sealed with vitreous enamel. The frictional resistance of a chromosiliconized layer was investigated under exposure to a corrosive medium of sugar slurry. Corrosion damage was examined with the use of a three-cylinder and cone wear tester.

The structure of the analyzed layers was evaluated by light and scanning microscopy, X-ray diffraction and glow discharge optical emission spectroscopy (GDOES). The thickness, surface roughness and hardness of samples were determined. Chromosiliconizing of C45 steel samples extended the life of friction elements in a sugar slurry environment.

Introduction

The design of machine elements requires solutions that improve operational efficiency. Various technologies for producing surface coatings are developed (BI 2009, KASPRZYCKA 2006, MŁYNARCZAK 2011, PERTEK 2003, ROHR 2005, WIERZCHOŃ 2010). On a highly competitive market, there is a demand for low-cost methods that guarantee the achievement of satisfactory operating parameters, including resistance to wear caused by friction and corrosion.

* Correspondence: Iwona Bauer, Katedra Technologii Materiałów i Maszyn, Uniwersytet Warmińsko-Mazurski, ul. Oczapowskiego 1, 10-736 Olsztyn, e-mail: iwona.bauer@uwm.edu.pl

Chromosiliconizing is a method that fulfills the above requirements. This process has been discussed at length by (AGARWAL 2007, HONCHI 2002, IGNATENKO 1991, NISHIMOTO 2003, NAKONIECZNY 2006). It is a relatively inexpensive technique for improving the working parameters of tools and machine parts. The attributes of chromosiliconized layers produced by gas and powder methods are enhanced through the selection of optimal mixture components, process parameters and carbon concentrations in steel.

Damage to machine components caused by tribocorrosion, corrosion or both processes poses a significant problem in many industries. This study analyzes the tribocorrosion of chromosiliconized layers, which remains poorly investigated (BAUER 2008, WEI 2000).

A sugar factory can increase its productive capacity by optimizing its technological processes, reducing its consumption of raw materials and energy, increasing its productive efficiency and maximizing the reliability of process lines. Sugar production machines are made of various materials, including those characterized by high resistance to wear and consequently, high cost which affects overall economic effectiveness. In modern sugar plants, machines are designed based on the latest technological solutions. Drum vacuum filters are replaced with membrane-chamber filter presses, and honeycomb steam chambers are introduced. In the sugar industry, many machines become damaged under exposure to corrosive media, mechanical load and friction, as discussed by (BURSTEIN 2000, BUCHANAN 2007, ZHENG 2000).

The aim of the work

The aim of this study was to investigate the frictional resistance of chromosiliconized steel samples under exposure to a corrosive medium of sugar slurry.

The object and methodology of the study

Samples of C45 steel were chromosiliconized by the powder-pack method. The chemical composition of steel given in the product's certificate is presented in Table 1. The process was carried out in a Labotherm LH15/14 furnace at 1000°C for 6 hours. The applied powder mix had the following composition: 70% ferrochromium powder enriched with SiC, 29.5% kaolin and 0.5% ammonium chloride (NH₄Cl). Samples of C45 steel were placed in the powder mix in special boxes made of X6CrNiTi18-10 steel. To prevent sample oxidation, the boxes were covered with lids and sealed with vitreous enamel which melts

at temperatures higher than 600°C. The boxes were placed in a furnace heated to process temperature. After the chromosiliconizing process, the first group of steel samples for tribocorrosion analysis was quenched in oil at 840°C and tempered at 500°C for 2 hours. The second group of steel samples was not subjected to heat treatment.

Table 1

Chemical composition of C45 steel (wt. %)

Steel grade	C	Si	Mn	S	P	Cr	Ni	Cu	Mo
C45	0.44	0.1	0.64	0.018	0.015	0.05	0.10	0.27	0.023

Microstructural analyses and thickness measurements of a chromosiliconized layer were carried out under the Olympus IX 70 metallographic microscope. Nital-etched microsections perpendicular to the surface of the sample were examined. The phase composition of a chromosiliconized layer was evaluated using a Philips X'Pert diffractometer with $\text{CuK}\alpha$ radiation and monochromatization of diffracted beams.

Chemical composition was determined by SEM with X-ray microanalysis and glow discharge optical emission spectroscopy (GDOES).

Surface roughness was measured with a Hommel Tester T1000. The following values were registered: R_a – arithmetic mean roughness deviation, R_z – height at ten roughness profile peaks, S_m – mean spacing of roughness profile peaks. Vickers hardness tests HV 0.05 were performed on transverse microsections using Reichert REF-2 and Zwick hardness testers.

The tribological properties of two groups of steel samples exposed to a corrosive medium were analyzed with the use of the I-47-K-54 wear tester consisting of three cylinders and a cone. A conical counter sample of C45 steel was enhanced to hardness level 48HRC. Linear wear was measured for 100 minutes (which corresponds to a distance of $s = 3470$ m) at friction velocity of 0.58 m/s and cone rotational speed of 576 rpm under the pressure of 50 MPa, 100 MPa, 200 MPa and 300 MPa. The corrosive medium was sugar slurry with $\text{pH} = 11.7$ and the following composition: 66.5% CaCO_3 , 3.5% MgCO_3 , 0.06% Na and 0.12% K. Sugar slurry was administered in the amount of 30 drops/minute.

Results and discussion

Chromosiliconizing resulted in gray and somewhat glossy surface. SEM image of the surface is presented in Figure 1.

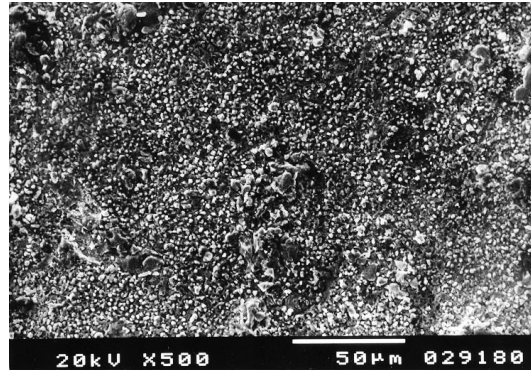


Fig. 1. Surface of C45 steel samples after chromosiliconizing, SEM, magnification 500×

Chromosiliconized layers on samples of C45 steel were characterized by higher surface roughness than uncoated steel. Roughness height was smaller than layer thickness. The results of surface roughness measurements are given in Table 2 and Figure 2.

Table 2
Stereometric parameters characterizing the surface topography of C45 steel samples with and without a chromosiliconized layer

Steel grade	R_a [μm]	R_z [μm]	S_m [μm]
C45 without surface layer	0.28	3.81	66.66
C45 after chromosiliconizing	0.58	4.34	100.0

The microstructure of a chromosiliconized layer on C45 steel was analyzed under a light microscope on transverse nital-etched microsections. A bright, non-etched layer with an estimated thickness of 16 μm was observed, and it was clearly separated from the steel substrate (Fig. 3).

X-ray diffraction of chromosiliconized layers revealed the presence of $(\text{Cr,Fe})_7\text{C}_3$ carbide and $\text{Cr}_2(\text{N,C})$ carbonitride. The estimated chemical composition of the layers determined by analysis was as follows: by weight 78% Cr, 12% Fe and 0.1% Si.

Vickers hardness tests (HV 0.05) (PN-EN ISO 6507-1:1999) performed on transverse microsections revealed a six-fold increase in hardness values to 1430 HV0.05 after chromosiliconizing. Hardness values are presented in Figure 4.

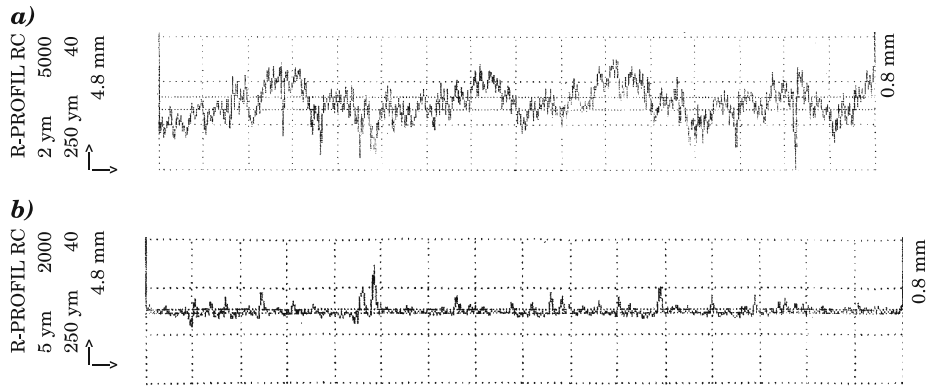


Fig. 2. The profilogram of the surface roughness of C45 steel samples with (b) and without (a) a chromosiliconized layer

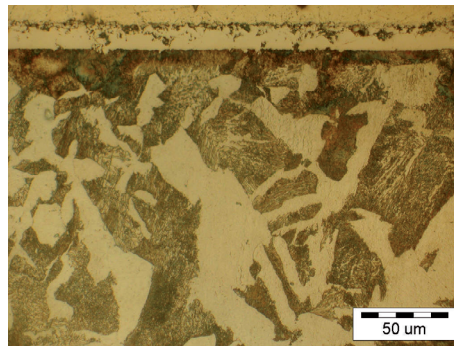


Fig. 3. Microstructure of C45 steel with a chromosiliconized layer. Light microscope, 500x magnification. Etched with nital

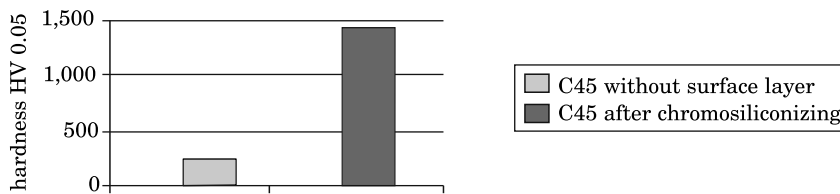


Fig. 4. Hardness of C45 steel samples

In frictional resistance tests under exposure to sugar slurry, chromosiliconized layers that had not been subjected to heat treatment at the first stage of the procedure (30 min) were characterized by loss of luster, and no signs of corrosion were observed. The examined layers underwent uniform wear at successive stages of the test under the pressure of 50 MPa, 100 MPa,

200 MPa. A pressure increase to 300 MPa led to accelerated wear, surface cracking and individual symptoms of uniform corrosion after 40 minutes of operation. Signs of non-uniform corrosion and frictional seizure were observed after 60 minutes. Linear wear was determined at $3.25\text{--}15.48\ \mu\text{m}$ during 10–100 minute tests carried out under the pressure of 50–200 MPa (Fig. 5).

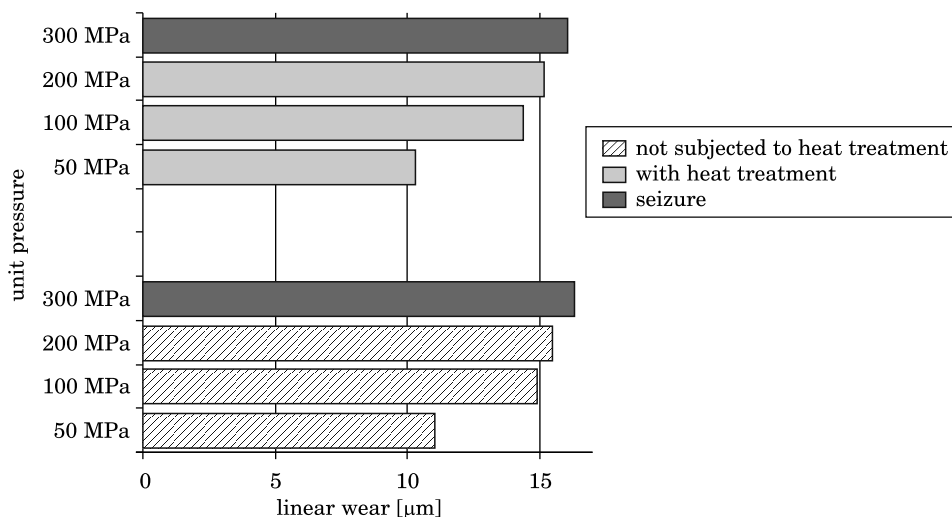


Fig. 5. Linear wear of C45 steel samples with chromosiliconized layers, at different unit pressure values in a sugar slurry environment

After 30 minutes of the friction test under exposure to sugar slurry, heat-treated chromosiliconized layers showed loss of luster but no signs of corrosion. No signs of accelerated wear were observed under the pressure of 50–200 MPa (linear wear $1.78\text{--}15.19\ \mu\text{m}$). Intensified wear was reported after 80 minutes of operation under the pressure of 300 MPa when surface cracking and uniform corrosion were noted. Surface pits were reported after 100 minutes. Under the pressure of 300 MPa wear depth exceeded layer thickness which led to frictional seizure. Linear wear was determined at $16.05\ \mu\text{m}$ (Fig. 5).

Conclusions

The study presents the results of an experiment investigating the tribocorrosion of chromosiliconized layers exposed to sugar slurry. Samples of C45 steel were chromosiliconized by the powder-pack method to produce a diffu-

sion layer with the thickness of 16 μm , containing mostly $(\text{Cr}, \text{Fe})_7\text{C}_3$ carbide and $\text{Cr}_2(\text{N}, \text{C})$ carbonitride.

Chromosiliconized steel samples were characterized by higher surface roughness than uncoated samples. The hardness of chromosiliconized samples increased six-fold, to 1430 HV0.05. In comparison with chromosiliconized layers that had not been subjected to heat treatment (linear wear $3.25 \pm 15.48 \mu\text{m}$) and heat-treated chromosiliconized layers on C45 steel samples, extended the life of friction elements in a sugar slurry environment under the pressure of 50–200 MPa (linear wear $1.78 \pm 15.19 \mu\text{m}$).

Under the pressure of 300 MPa, wear depth exceeded layer thickness which led to frictional seizure.

Translated by ALEKSANDRA POPRAWKA

References

- AGARWAL S., JAIN A., LAL C., GANESAN V., JAIN I.P. 2007. *Surface morphology and phase formation at Cr/Si system*. Applied Surface Science, 253(10): 4721–4726.
- BI Q., LIU W., MA J., YANG J., PU Y., XUE Q. 2009. *Tribocorrosion behavior of Ni-17.5Si-29.3 Cr alloy in sulfuric acid solution*. Tribology International, 42(7): 1081–1087.
- BAUER I. 2008. *The effect of microstructure on the tribocorrosive properties of chromosiliconized layers*. Physico-Chemical Mechanics of Materials, 7: 293–295.
- BUCHANAN V.E., SHIPWAY P.H., MC CARTNEY D.G. 2007. *Microstructure and abrasive wear behaviour of shielded metal arc welding hardfacings used in the sugarcane industry*. Wear, 263(1–6): 99–110.
- BURSTEIN G.T., SASAKI K. 2000. *Effect of impact angle on the slurry erosion-corrosion of 304L stainless steel*. Wear, 240: 80–94.
- HONCHI M., YAMAZAKI T. 2002. *Chromium/silicon composite pack cementation agent and treatment using the same*. Patent JP 2002129304.
- IGNATENKO P.I., KUDELIN YU.V., GONCHAROV A.A., MUZA M.A. 1991. *The influence of nitrogen content and resistive chromosilicon films thickness on their corrosion resistance*. Fizyko-Chimicheskaja Mechanika Materialov, 27(5): 102–103.
- KASPRZYCKA E., SENATORSKI J. 2006. *Structure and tribological properties of carbide layers produced in vacuum chromizing process*. Tribologia, 3: 87–93.
- MEYNARCZAK A., PIASECKI A. 2011. *Dyfuzyjne manganowanie żelaza*. Inżynieria Materiałowa, 4: 597–599.
- NAKONIECZNY A., BAUER I. 2006. *Factors affecting corrosion resistance of chromium-silicon diffusion layers*. Conference “Balttechmasz”, Kaliningrad (Russia), p. 420–424.
- NISHIMOTO A., AKAMATSU K., NAKAO K., ICHNI K., IKE K. 2003. *High temperature properties of chromosiliconized stainless steels*. International Surface Engineering Congress-proceedings of the 1 st Congress, Columbus, p. 246–249.
- PERTEK A., KULKA M. 2003. *Microstructure and properties of composite (B+C) diffusion layers on low-carbon steel*. Journal of Materials Science, 38: 269–273.
- ROHR V., DONCHEV A., SCHTZE M., MILEWSKA A., PEREZ F.J. 2005. *Diffusion coatings for high temperature corrosion protection of 9–12% Cr steels*. Corrosion Engineering Science and Technology, 40(3): 226–232.
- WIERZCHOŃ T., SZAWŁOWSKI J. 2010. *Inżynieria powierzchni a potrzeby materiałowe przemysłu*. Materiały XIII Seminarium Grupy SECO/WARWICK, Świebodzin, p. 5–15.

- WIERZCHOŃ T., ULBIN-POKORSKA I., SIKORSKI K. 2000. *Corrosion resistance of chromium nitride and oxynitride layers produced under glow discharge conditions*. Surface and Coatings Technology, 130(2-3): 274-279.
- WEI P., WAN X.R. 2000. *The effect of coating heat treatment on Cr-Si and heat treatment on mechanical properties of Cr17Ni2 stainless steel*. Surface and Coating Technology, 132: 137-142.
- ZHENG Y.G., YAO Z.M., KE W. 2000. *Erosion-corrosion resistant alloy development for aggressive slurry flows*. Materials Letters, 46: 362-368.
- PN-EN ISO 6507-1:1999. *Metallic materials-Vickers hardness test. Part 1: Test method*.
- PN-H-04302:1983. *The strength tests of metals. The friction test in 3 rollers-cone system*.

THE BASIC CLOSURES OF FLUID MECHANICS IN FORM CHARACTERISTIC FOR THE FINITE VOLUME METHOD

*Wojciech Sobieski**

Department of Mechanics and Machine Design
University of Warmia and Mazury in Olsztyn

Received 9 November 2012; Accepted 24 April 2013; Available on line 15 July 2013

Key words: Finite Volume Method, balance equations, closures.

Abstract

This short article presents all basic “closures” that are needed to supplement the general set of balance equations in form characteristic for the Finite Volume Method. In subsequent chapters the equation of state, viscous molecular stress tensor, turbulent stress tensor, molecular heat flux, turbulent heat flux and momentum and energy sources were described. This article is a second part of a cycle dedicated for the mathematical basis of Finite Volume Method. The motivation for writing the article follows from the observation that the Finite Volume Method is usually described in greater detail in monographic books, or very briefly in the basic books dedicated to fluid mechanics. This article is an attempt to center justifications of these approaches, so that in the simplest way show the readers the basic knowledge of the so-called Computational Fluid Mechanics. For this reason this article can be treated as a literature review.

Introduction

The basic set of balance equations in Finite Volume Method, described in article (SOBIESKI 2011), has a form:

$$\left\{ \begin{array}{l} \frac{\partial \rho}{\partial t} + \operatorname{div}(\rho \vec{v}) = 0 \\ \frac{\partial(\rho \vec{v})}{\partial t} + \operatorname{div}(\rho \vec{v} \vec{v} + p \vec{I}) = \operatorname{div}(\vec{\tau}^m + \vec{\tau}^R) + \rho s_b \\ \frac{\partial(\rho e)}{\partial t} + \operatorname{div}(\rho e \vec{v} + p \vec{I} \vec{v}) = \operatorname{div}[(\vec{\tau}^m + \vec{\tau}^R) \vec{v} + \vec{q}^m + \vec{q}^R] + \rho s_e \end{array} \right. \quad (1)$$

* Correspondence: Wojciech Sobieski, Katedra Mechaniki i Podstaw Konstrukcji Maszyn, Uniwersytet Warmińsko-Mazurski, ul. M. Oczapowskiego 11, 10-957 Olsztyn, tel. +48 89 523-32-40, e-mail: wojciech.sobieski@uwm.edu.pl

where:

- ρ – density [kg/m³],
- \vec{v} – velocity [m/s],
- p – static pressure [Pa],
- \vec{I} – unit tensor [-],
- $\vec{\tau}^m$ – viscous molecular stress tensor [Pa],
- $\vec{\tau}^R$ – turbulent Reynolds stress tensor [Pa],
- s_b – source of forces [N/m³],
- e – the sum of kinetic and internal energy [J/kg],
- \vec{q}^m – molecular heat flux [J/(m² · s)],
- \vec{q}^R – turbulent heat flux [J/(m² · s)],
- s_e – sources of heat [J/(m³ · s)].

The set of balance (or transport) equations (1) is not complied and need to be supplemented by many “closures”, this means a specific models describing the individual issues. In current article, the basic “closures” for the equation of state, stress tensors, heat transfer and sources are described. It is a direct continuation of the article (SOBIESKI 2011) and for this reason, the introduction is limited to the minimum. The motivation of this work was a desire to prepare a short and clear introduction to the mathematical model characteristic for the Finite Volume Method (FVM). This follows from the observation that the mathematical model characteristic for the FVM is usually described in greater detail in monographic books, or very briefly in the basic books dedicated to fluid mechanics. This article stems from a desire of averaging these approaches.

Equation of state

The equation of state is a constitutive equation which provides a mathematical relationship between basic quantities in a system such as temperature, pressure and volume. Equations of state are useful in describing the properties of fluids (gases and liquids), mixtures of fluids and even solids. The formula depends on the adopted model of the matter, but must be added to the set (1) in any case as a separate equation. In the literature, one can find many different equations of state; the most common one known is the Clapeyron’s equation (BADUR 2005).

$$pV_m = RT \tag{2}$$

where:

- p – the static pressure [Pa],
- V_m – the volume of 1 mole of gas or liquid [m³],
- R – ideal gas constant equal to 8.314472 [J/(mol · K)],
- T – the temperature [K].

The formula (2) is dedicated for ideal gases; for real gases more appropriate is the Van der Waals equation (WAALS 1910)

$$\left(p + \frac{a}{V_m^2}\right) (V_m - b) = RT \quad (3)$$

where:

a and b are substance-specific constants, taking into account the pressures arising from gas particle vibration and its volume, respectively. In the literature, one can find other formulas for the equation of state, too.

In the case of the liquid flows, it is often assumed that

$$\begin{cases} \rho = \text{const.} \\ u = \text{const.} \end{cases} \quad (4)$$

where:

ρ – is the liquid density [kg/m^3],

u – is the internal energy [J].

Viscous molecular stress tensor

The viscous molecular stress tensor $\hat{\tau}^m$ is one of the important closures in set of equations (1). The form of this tensor depends on the adopted model of fluid. In the numerical analysis is usually adopted the Pascal's model, Newton's model or a non-Newtonian fluid model. The Pascal's model assumes existence of a stress only in perpendicular direction, without taking into account the viscosity and compressibility. In this case $\hat{\tau}^m = 0$. The Pascal's model can be used for ideal gases.

The most popular in the practice is the Newton's model, which may be used in modeling flows of air, water, oil and a lot of other fluids with a simple molecular structure (PUZYREWSKI, SAWICKI 2000). In this model the stress (τ^m) versus strain rate ($\dot{\gamma}$) curve is linear and passes through the origin (Fig. 1a). For one direction flow and Cartesian coordinates (Fig. 1b), it can be written as (PUZYREWSKI, SAWICKI 2000, GRYBOŚ 1998)

$$\tau_{xy}^m = \mu_l \frac{\partial v_x}{\partial y} \quad (5)$$

where:

μ_l – is the constant of proportionality called dynamic viscosity [$\text{Pa} \cdot \text{s}$].

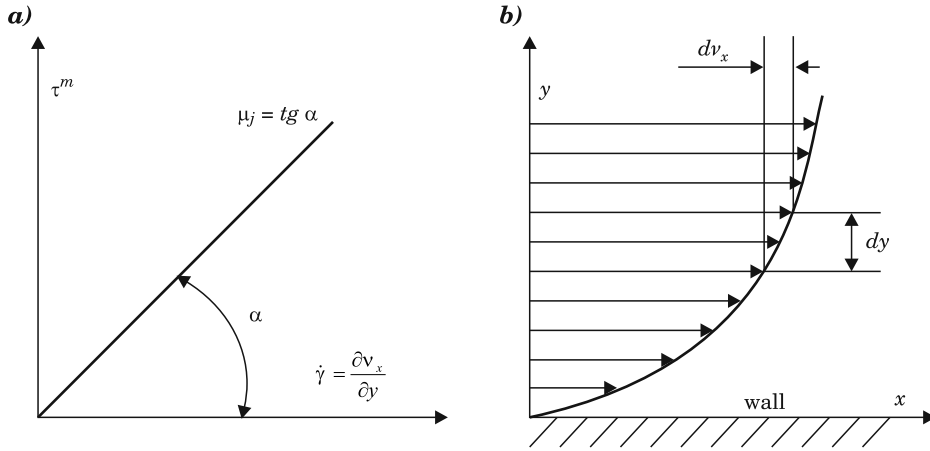


Fig 1. Relationship between stress and strain rate for Newtonian fluid

In general cases, the total stress tensor $\overset{\leftrightarrow}{T}$ for Newtonian fluid may be written in form

$$\overset{\leftrightarrow}{T} = a\overset{\leftrightarrow}{I} + b\overset{\leftrightarrow}{D} \tag{6}$$

where:

a and b are the model constants,

$\overset{\leftrightarrow}{I}$ – is the unit tensor,

$\overset{\leftrightarrow}{D}$ – is the deformation rate tensor.

The first part describes the stress in perpendicular direction, and the second part takes into account the friction caused by viscosity; tensor $\overset{\leftrightarrow}{D}$ is here a three dimensional counterpart of the quotient appearing in the equation (5). In Cartesian coordinates this tensor has a form as follow (PUZYREWSKI, SAWICKI 2000)

$$\overset{\leftrightarrow}{D} = \begin{bmatrix} \frac{\partial v_x}{\partial x} & \frac{1}{2} \left(\frac{\partial v_x}{\partial y} + \frac{\partial v_y}{\partial x} \right) & \frac{1}{2} \left(\frac{\partial v_x}{\partial z} + \frac{\partial v_z}{\partial x} \right) \\ \frac{1}{2} \left(\frac{\partial v_x}{\partial y} + \frac{\partial v_y}{\partial x} \right) & \frac{\partial v_y}{\partial y} & \frac{1}{2} \left(\frac{\partial v_y}{\partial z} + \frac{\partial v_z}{\partial y} \right) \\ \frac{1}{2} \left(\frac{\partial v_x}{\partial z} + \frac{\partial v_z}{\partial x} \right) & \frac{1}{2} \left(\frac{\partial v_y}{\partial z} + \frac{\partial v_z}{\partial y} \right) & \frac{\partial v_z}{\partial z} \end{bmatrix} \tag{7}$$

Therefore, the formula (6) can be written in form

$$\overset{\leftrightarrow}{T} = \begin{bmatrix} a & 0 & 0 \\ 0 & a & 0 \\ 0 & 0 & a \end{bmatrix} + \begin{bmatrix} b \frac{\partial v_x}{\partial x} & b \frac{1}{2} \left(\frac{\partial v_x}{\partial y} + \frac{\partial v_y}{\partial x} \right) & b \frac{1}{2} \left(\frac{\partial v_x}{\partial z} + \frac{\partial v_z}{\partial x} \right) \\ b \frac{1}{2} \left(\frac{\partial v_x}{\partial y} + \frac{\partial v_y}{\partial x} \right) & b \frac{\partial v_y}{\partial y} & b \frac{1}{2} \left(\frac{\partial v_y}{\partial z} + \frac{\partial v_z}{\partial y} \right) \\ b \frac{1}{2} \left(\frac{\partial v_x}{\partial z} + \frac{\partial v_z}{\partial x} \right) & b \frac{1}{2} \left(\frac{\partial v_y}{\partial z} + \frac{\partial v_z}{\partial y} \right) & b \frac{\partial v_z}{\partial z} \end{bmatrix} \quad (8)$$

On the other hand

$$\overset{\leftrightarrow}{T} = \begin{bmatrix} T_{xx} & T_{xy} & T_{xz} \\ T_{yx} & T_{yy} & T_{yz} \\ T_{zx} & T_{zy} & T_{zz} \end{bmatrix} \quad (9)$$

Two tensors are the same, if their invariants are equal, then

$$T_{xx} + T_{yy} + T_{zz} = 3a + b \left(\frac{\partial v_x}{\partial x} + \frac{\partial v_y}{\partial y} + \frac{\partial v_z}{\partial z} \right) \quad (10)$$

The expression in brackets describes divergence of the velocity, then

$$T_{xx} + T_{yy} + T_{zz} = 3a + b \operatorname{div}(\vec{v}) \quad (11)$$

After dividing both sides by 3, we obtain

$$\frac{T_{xx} + T_{yy} + T_{zz}}{3} = a + \frac{1}{3} b \operatorname{div}(\vec{v}) \quad (12)$$

The equation describes the average stress perpendicular to the surface – it is the static pressure p (SONIN 2001) (the minus sign results from the orientation of the surface versor), then

$$-p = a + \frac{1}{3} b \operatorname{div}(\vec{v}) \quad (13)$$

From the above equation, one can designate the constant a :

$$a = -p - \frac{1}{3} b \operatorname{div}(\vec{v}) \quad (14)$$

The constant b can be derived by comparison of the T_{xy} component from tangential part of stress tensor formula (8) with the classical form (5), for one direction flow (when $v_y = v_z = 0$)

$$\mu_l \frac{\partial v_x}{\partial y} = b \frac{1}{2} \frac{\partial v_x}{\partial y} \quad (15)$$

and

$$b = 2\mu_l \quad (16)$$

The constants a and b can be included to the formula (6):

$$\overleftrightarrow{T} = -p\overleftrightarrow{I} + 2\mu_l \overleftrightarrow{D} - \frac{2}{3} \mu_l \operatorname{div}(\vec{v}) \overleftrightarrow{I} \quad (17)$$

or in another form

$$\overleftrightarrow{T} = -p\overleftrightarrow{I} + \overleftrightarrow{\tau}^m \quad (18)$$

where

$$\overleftrightarrow{\tau}^m = 2\mu_l \overleftrightarrow{D} - \frac{2}{3} \mu_l \operatorname{div}(\vec{v}) \overleftrightarrow{I} \quad (19)$$

In set of equations (1), the pressure part is transferred to the right side, so as to obtain the separation of convection and diffusion (it was discussed in the previous article (SOBIESKI 2011)).

In flows of very rapid change in velocity (e.g. flows with shock waves) the tensor $\overleftrightarrow{\tau}^m$ needs a correction. The part $-\frac{2}{3} \mu_l$ is replaced by $-\frac{2}{3} \mu_l + \mu_l'$, where μ_l' is the second viscosity or volumetric viscosity (SONIN 2001, Fluent 6.3. User's Guide 2006).

$$\overleftrightarrow{\tau}^m = 2\mu_l \overleftrightarrow{D} - \frac{2}{3} \mu_l \operatorname{div}(\vec{v}) \overleftrightarrow{I} + \mu_l' \operatorname{div}(\vec{v}) \overleftrightarrow{I} \quad (20)$$

Formula (20) is the general formula of viscous molecular stress tensor for Newtonian fluid used to supplement the basic set of equations (1). For non-Newtonian fluid, a different stress tensor must be defined, appropriate to the property of the fluid. In the literature, one can find tens of different models. General non-Newtonian fluids are divided into a few groups due to the relationship between stress and strain rate tensor (Fig. 2a) and on two groups due to the change of the properties at the time (Fig 2b). A more extensive discussion of this issue does not fall within the scope of this article.

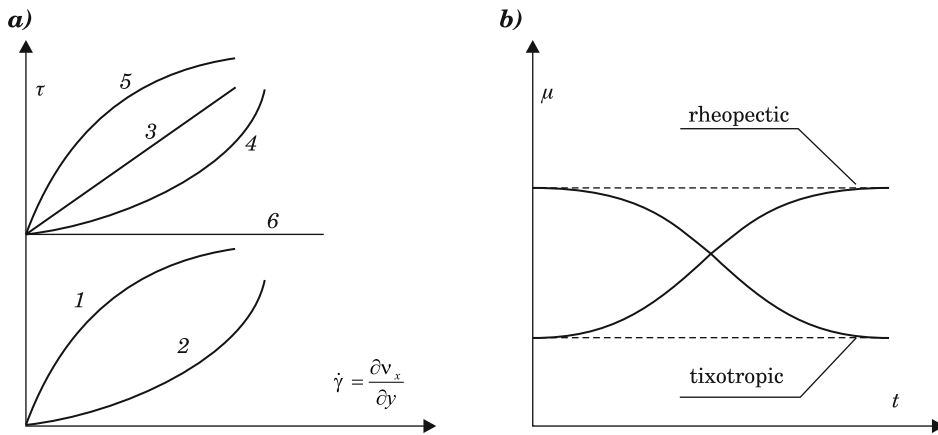


Fig 2. Types of non-Newtonian fluid: 1 – pseudoplastic fluid, 2 – dilatant fluid, 3 – Bingham fluid, 4 – dilatant fluid with yield, 5 – pseudoplastic fluid with yield, 6 – ideal pseudoplastic fluid

Turbulent stress tensor

Turbulence modeling is one of the biggest problems of modern fluid mechanics. In the CFD area, it can be at present to distinguish a few basic approaches to the turbulence modeling (Fig. 3).

Direct Numerical Simulation (DNS) (MOIN 1998, JOSEPH 2005, BOGUSŁAWSKI 2008). It is the most accurate numerical method to solve turbulent flows. In this method all spatial and temporal scales (Fig. 4) are resolved. Hence, computed results are equivalent to those that are obtained experimentally. The disadvantage of the method is enormous computing power requirements – the cost of a simulation goes up to in term of CPU time. Currently, the method can be used only for flows with relatively low Reynolds number.

Large Eddy Simulation (LES) (PIOMELLI et al. 2000, UYGUN et al. 2004). The essence of this method is the division of eddies on the large scale and the subgrid scale, according to the Kolmogorov's theorem (PUZYREWSKI,

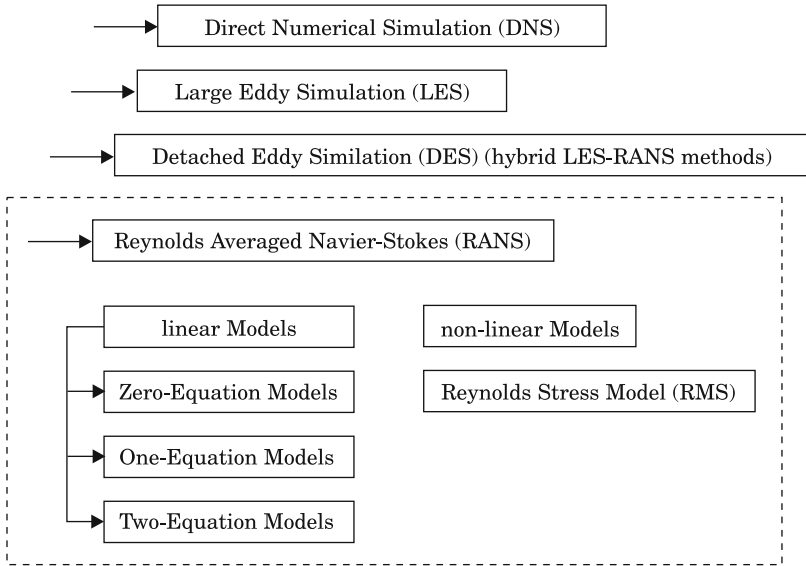


Fig 3. The main group of turbulence models
 Source: KACZYŃSKI (1997), UYGUN et al. (2004), SAAD (2011).

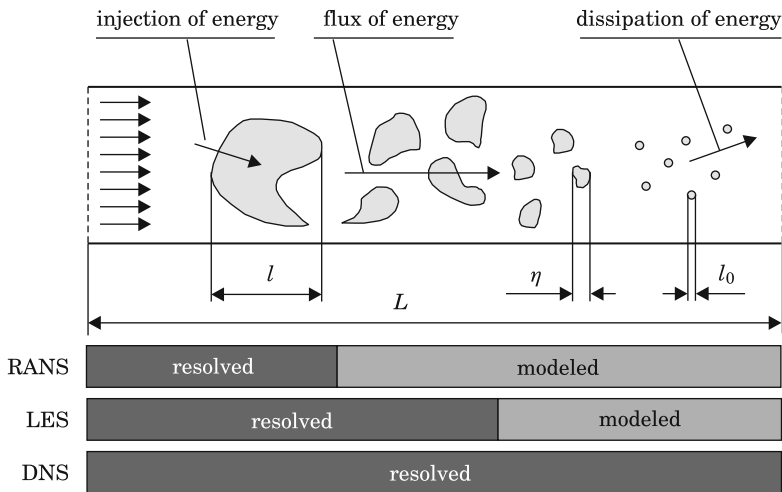


Fig 4. Scales of the eddies in turbulent flow

SAWICKI 2000), and next treating both scales separately. This concept follows from the observation that in flows with sufficiently high Reynolds number largest and smallest scales are well separated: the energy of the main flow passes through the mechanism of vortex-stretching and the decay of vortices to an ever smaller scale (Fig. 4). LES allows to obtain the explicitly result for

the large eddies in a calculation and implicitly solution for the small eddies by using a subgrid scale model (the principal operation in LES is low-pass filtering). For this reason, LES allows better fidelity than alternative approaches (RANS methods) that do not resolve any scales of the solution. This method requires greater computational resources than RANS methods, but is far cheaper than DNS.

Detached Eddy Simulations (DES) (SPALART et al. 2006). It is a mix of a RANS and LES models. Regions near solid boundaries and where the turbulent length scale is less than the maximum grid, dimensions are assigned the RANS mode of solution. As the turbulent length scale exceeds the grid dimension, the regions are solved using the LES mode. Therefore the grid resolution for DES is not as demanding as pure LES, thereby considerably cutting down the cost of the computation. The disadvantage of this method is that the grid generation is more complicated than for a simple RANS or LES.

Reynolds Averaged Navier-Stokes (RANS) models (EASOM 2000, FLUENT 6.3 User's Guide 2006). It is the oldest and most popular approach to the turbulence modeling in CFD area – for this reason, the approach is described here in more detail. In RANS concept, the conservation equations are time-averaged, according to the velocity decomposition proposed by Reynolds (CELIK 1999, ADRIAN et al. 2000, PUZYREWSKI, SAWICKI 2000). In this decomposition, the current value of velocity consists of an average velocity \bar{v} and a fluctuation v' (Fig. 5).

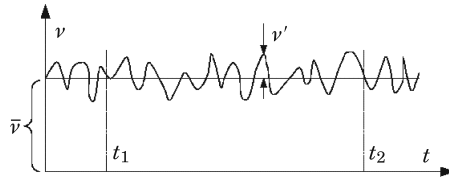


Fig 5. The idea of velocity decomposition

The velocity decomposition may be written as follow:

$$\bar{v} = \frac{1}{t_2 - t_1} \int_{t_1}^{t_2} v dt \quad (21)$$

wherein

$$\frac{1}{t_2 - t_1} \int_{t_1}^{t_2} v' dt = 0 \quad (22)$$

and

$$\frac{1}{t_2 - t_1} \int_{t_1}^{t_2} v'v' dt = \overline{v'v'} \quad (23)$$

The decomposition idea can be introduced to the Navier-Stokes equation (i.e. to the momentum equation without the turbulence member), and therefore

$$\frac{\partial}{\partial t} (\rho(\bar{v} + v')) + \text{div}(\rho(\bar{v} + v')(\bar{v} + v') + \overset{\leftrightarrow}{p}I) = \text{div}(\overset{\leftrightarrow}{\tau}^m) + \rho s_b \quad (24)$$

or

$$\frac{\partial}{\partial t} (\rho(\bar{v} + v')) + \text{div}(\rho(\bar{v}\bar{v} + \bar{v}v' + v'\bar{v} + v'v') + \overset{\leftrightarrow}{p}I) = \text{div}(\overset{\leftrightarrow}{\tau}^m) + \rho s_b \quad (25)$$

Taking into account the relationships (22) and (23) in the above equations, receives a shorter form

$$\frac{\partial}{\partial t} (\rho\bar{v}) + \text{div}(\rho\bar{v}\bar{v} + \overset{\leftrightarrow}{p}I) = \text{div}(\overset{\leftrightarrow}{\tau}^m - \overline{\rho v'v'}) + \rho \vec{s}_b \quad (26)$$

where the member $\overline{\rho v'v'}$ (in equation (26) moved to the right side) is the general record of the turbulent stress tensor (DROBNIAK et al. 2008).

$$\overset{\leftrightarrow}{\tau}^R = \begin{vmatrix} -\rho v_x v_x & -\rho v_x v_y & -\rho v_x v_z \\ -\rho v_y v_x & -\rho v_y v_y & -\rho v_y v_z \\ -\rho v_z v_x & -\rho v_z v_y & -\rho v_z v_z \end{vmatrix} \quad (27)$$

In the current approach, the turbulent stress tensor is treated as a “correction” of viscous molecular stress tensor $\overset{\leftrightarrow}{\tau}^m$, which must be added into turbulent flows. This conception is often called the Boussinesq hypothesis or the Boussinesq approximation. The turbulent stress tensor has in this concept the same structure as the viscous molecular tensor

$$\overset{\leftrightarrow}{\tau}^R = 2\mu_t \overset{\leftrightarrow}{D} - \frac{2}{3}\mu_t \text{div}(\vec{v}) \overset{\leftrightarrow}{I} + \mu_t' \text{div}(\vec{v}) \overset{\leftrightarrow}{I} \quad (28)$$

but the dynamic viscosity μ_l is replaced by its turbulent counterpart μ_t . Now the total stress tensor may be noted as

$$\overleftrightarrow{\tau}^t = \overleftrightarrow{\tau}^m + \overleftrightarrow{\tau}^R = 2\mu_{eff} \overleftrightarrow{D} - \frac{2}{3}\mu_{eff} \text{div}(\vec{v}) \overleftrightarrow{I} + \mu'_{eff} \text{div}(\vec{v}) \overleftrightarrow{I} \quad (29)$$

where effective viscosity is defined as

$$\mu_{eff} = \mu_l + \mu_t \quad (30)$$

It is important, that μ_t is not a physical quantity, only a correction factor of μ_l . Usually it is assumed that this ratio depends on the kinetic energy of turbulence

$$k = \frac{1}{2} \overline{v_i v_i} \quad (31)$$

and its dissipation (denoted often as ε or ω). In the RANS approach, very often it is assumed that the turbulent viscosity depends on the distance of the wall. Another value is assumed in the boundary layer and another in the rest of the flow (KACZYŃSKI 1997).

Most popular models from the RANS group are shown in Fig. 6 (KACZYŃSKI 1997, VOIGT et al. 2003, ABDOL-HAMID et al. 2006, KARVINEN, AHLSTEDT 2008). On this figure, the linear models are divided due to the number of evolution equations needed to determine the value of μ_t , which must be added to the main set of equation (1) and which have the same mathematical structure, matched to the vector form of the balance equations. It is worth mentioning that in the literature are known models with a much larger number of evolution equations.

The equation (1) – and all derivation, which was shown in work (SOBIESKI 2011) – has the form typical for RANS methods. Using other methods require additional mathematic transformations of the set (1). In RANS methods, the members associated with turbulence are there treated as correction factors of parts describing laminar flows. After this adjusting, the results of calculations agree better with experiments, but only if the turbulence model is chosen correctly.

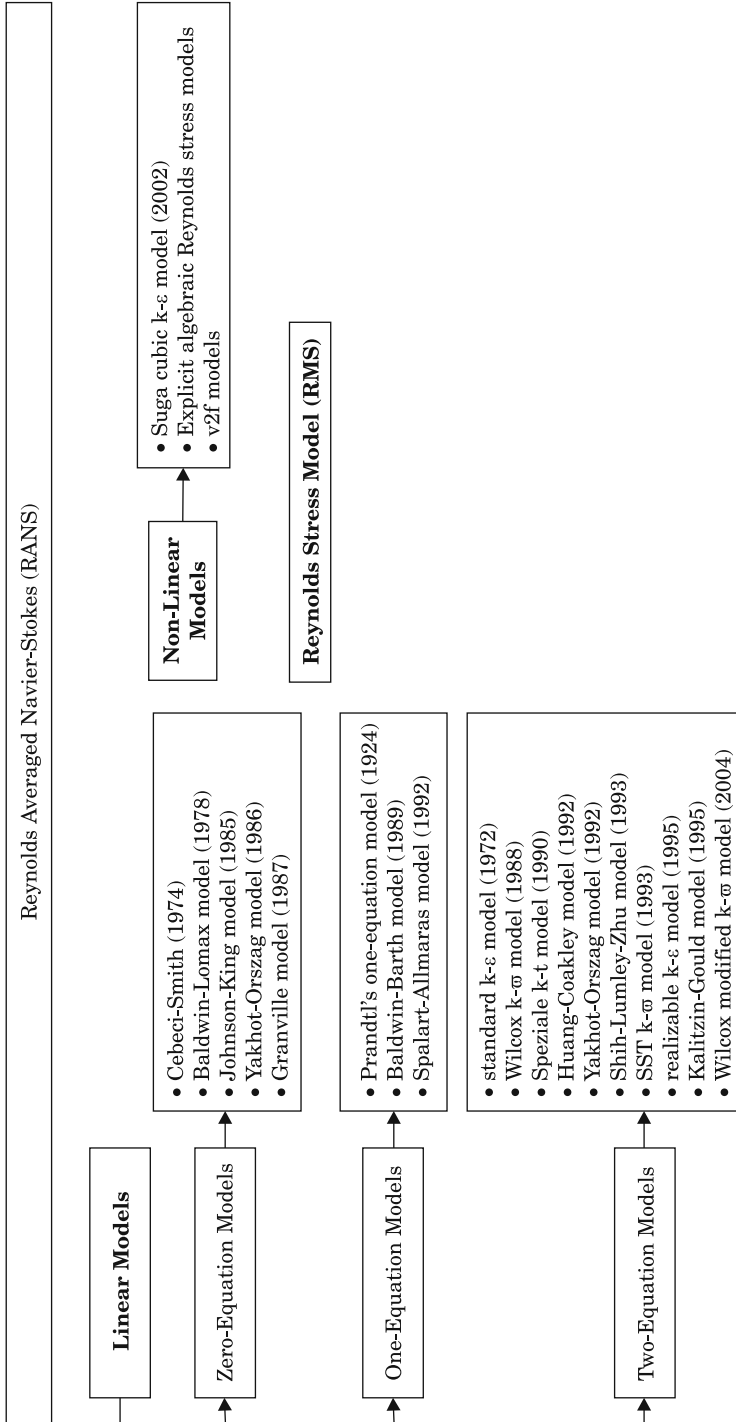


Fig. 6. The most popular models from the RANS group

Molecular and turbulent heat flux

The molecular heat flux in set of equations (1) can be calculated on basis the Fourier Law (MAGAGNATO 1998, STANISZEWSKI 1998, WRÓBLEWSKI 2008).

$$\vec{q}^m = -\lambda_l \cdot \text{grad}(T) \quad (32)$$

where:

λ_l – is the material's conductivity appropriate for laminar flows [W/(m · K)].

In the literature, it is assumed that a positive sign applies to the effluent stream from the volume, hence the negative sign in the formula. In the case of turbulent flow, one can exploit the concept of a correction factor (analogy like in the formula (29)), then

$$\vec{q}^t = \vec{q}^m + \vec{q}^R = \lambda_{eff} \cdot \text{grad}(T) \quad (33)$$

where effective material's conductivity is defined as

$$\lambda_{eff} = \lambda_l + \lambda_t \quad (34)$$

In this formula, λ_t is the material's conductivity appropriate for turbulent flows.

Momentum and energy sources

In case of one phase flow, the source vector is very simple. The momentum inside a control volume can be change only by the force of gravity, wherein this is important in principle, only for liquid flows. Effect of gravity, in the case of gas, is small and in most cases it can be neglected. The momentum source can therefore have a form

$$s_b = \pm g \quad (35)$$

where the sign depends on the orientation of the adopted coordinate system. The g is equal to the acceleration of objects under influence of the gravitational field [m/s²].

In case of flows without chemical reaction and phase change (which would require the existence in flow of several phases), the source of energy is always equal to zero.

Summary

This article presents basic information on the closures of balance equations, mass, momentum and energy in the form characteristic for the FVM and one phase flows. This information is very general in nature, but should orient the reader to the basic aspects of CFD. Unfortunately, the correct selection of the closures is a matter of a relatively difficult concept, requiring considerable knowledge and experience. Particularly troublesome is the determination of closure on the viscous stress tensor of non-Newtonian fluids and the closure describing the turbulence. It may indeed happen that laminar flow is analyzed, or those where the turbulence does not significantly affect the course of the modeled phenomenon, but in many cases, the choice of appropriate turbulence model is a key issue if we want to obtain quantitative agreement of calculation results with the experiment. Examples are flows in diffusers, ducts with plenty of walls or any type of flows around an object.

The issue relating to the closures is more complicated in cases with multiphase flows. It should then determine again the viscous and turbulent stress tensors of such a medium (we're talking about RANS approach), as well as numerous closures, describing interactions between phases: the exchange of mass, momentum and energy. These closures are dependent on many factors so that the final models describing two different situations of flow can be quite dissimilar to each other.

Translated by WOJCIECH SOBIESKI

References

- ABDOL-HAMID K.S., PAO S.P., HUNTER C.A., DEERE C.A. 2006. *PAB3D Its History in the Use of Turbulence Models in the Simulation of Jet and Nozzle Flows*. 44th AIAA Aerospace Sciences Meeting and Exhibit, 9–12 January 2006, Reno, Nevada, United States.
- ADRIAN R.J., CHRISTENSEN K.T., LIU Z.C. 2000. *Analysis and interpretation of instantaneous turbulent velocity field*. *Experiments in Fluids*, 29(3): 275–290.
- BADUR J. 2005. *Five lectures on modern thermomechanics fluid*. Lectures for Students, on-line, <http://www.imp.gda.pl/struktura/o2/z3/publications/wyklady/piecowykladow.pdf> (access: May 19, 2011).
- BOGUSŁAWSKI A., DROBNIAK S., TYLISZCZAK A. 2008. Turbulence – from randomness to the determinism. *Engineering Modeling*, 36: 41–48.
- CELIK I.B. 1999. *Introductory Turbulence Modeling. Lectures Notes*. West Virginia University in Morgantown, Mechanical & Aerospace Engineering Dept., United States.
- DROBNIAK S., BOGUSŁAWSKI A., TYLISZCZAK A. 2008. *Some Remarks on Modelling and Simulation of Turbulence*. *Journal Of Theoretical And Applied Mechanics*, 46(2): 243–256.
- EASOM G. 2000. *Improved Turbulence Models for Computational Wind Engineering*. PhD Thesis. University of Nottingham, United Kingdom.
- Fluent 6.3 User's Guide. Fluent Inc., September 2006.
- GRYBÓŚ R. 1998. *Fundamentals of fluid mechanics*. PWN, Warsaw.

- JOSEPH D. 2005. *Interrogations of Direct Numerical Simulation of Solid-Liquid Flows*. On-line, Fluid Book, http://www.efluids.com/efluids/books/efluids_books.htm (access: May, 19, 2011).
- KACZYŃSKI J. 1997. Review of major models of turbulence in computational programs to solve the Reynolds equations. *IMP PAN Scientific Issue*, 486(1448): 27–50.
- KARVINEN A., AHLSTEDT H. 2008. *Comparison of turbulence models in case of three-dimensional diffuser*. Proceedings of Open Source CFD International Conference, Berlin, Germany, 4–5 December, p. 17.
- MAGAGNATO F. 1998. *Kappa – Karlsruhe parallel program for aerodynamics*. *Task Quarterly*, 2: 215–270.
- MOIN P., MAHESH K. 1998. *Direct Numerical Simulation: A Tool In Turbulence Research*. *Annual Review of Fluid Mechanics*, 32: 539–578.
- PIOMELLI U., SCOTTI A., BALARAS E. 2000. *Large-eddy simulation of turbulent flows: from desktop to supercomputer*. In *Vector and Parallel Processing – VECPAR 2000*. (Springer: Berlin), p. 551–577.
- PUZREWICKI R., SAWICKI J. 2000. *Fundamentals of fluid mechanics and hydraulics*. PWN, Warsaw.
- SAAD T. 2011. *Turbulence Modeling for Beginners*. On-line, http://www.cfd-online.com/W/images/3/31/Turbulence_Modeling_For_Beginners.pdf (access: May, 24, 2011).
- SOBIESKI W. 2011. *The basic equations of fluid mechanics in form characteristic of the finite volume method*. *Technical Sciences*, 14(2): 299–313.
- SONIN A.A. 2001. *Fundamental Laws of Motion For Particles, Material Volumes and Control Volumes*. Lecture notes Massachusetts Institute of Technology, United States, on-line, http://web.mit.edu/2.25/www/pdf/fundamental_laws.pdf (access: May 27, 2011).
- STANISZEWSKI B. 1978. *Thermodynamics*. PWN, Warsaw.
- SPALART P.R., DECK S., SHUR M. L., SQUIRES K.D., STRELETS M.KH., TRAVIN A. 2006. *A new version of detached-eddy simulation, resistant to ambiguous grid densities*. *Theoretical And Computational Fluid Dynamics*, 20: 181–195.
- UYGUN M., ONBASIOGLU S., AVCI S. 2004. *Turbulence Medeling for Computational Fluid Dynamic, Part I: Conceptual Outlook*. *Journal of Areonautic and Space Technologies*, 1(4): 19–26.
- VAN DER WAALS J.D. 1910. *The equation of state for gases and liquids*. Nobel Lecture, December 12.
- VOIGT L.K., SÖRENSEN J.N., PEDERSEN J.M., BRÖNS M. 2003. *Review of Four Turbulence Models Using Topology*. Eighth International IBPSA Conference Eindhoven, Netherlands, August 11–14.
- WRÓBLEWSKI W. 2000. *Numerical simulation of flow phenomena in thermal turbines*. *Silesian University of Technology, Energetics*, 132: 9–214.

TWO MATHEMATICAL FORMULAS FOR ASSESSING SEED SEPARATION EFFICIENCY

*Zdzisław Kaliniewicz**

Department of Heavy Duty Machines and Research Methodology
University of Warmia and Mazury in Olsztyn

Received 8 March 2013; Accepted 10 March 2013; Available on line 15 July 2013

Key words: seeds, separation process, indicators, comparison.

Abstract

Two mathematical formulas for assessing the efficiency of seed mixture separation were analyzed. Increases in the crop seed yield and the efficiency of impurity separation were accompanied by higher seed separation efficiency regardless of the adopted formula. One of the examined formulas carried more information, and it could be used to determine the improvement in the purity of the separated product relative to the raw material. The difference in the analyzed formulas' ability to determine the efficiency of seed separation was minimized when the separation process was more efficient, i.e. when the value of partial indicators of separation efficiency was closer to 1. Both formulas could be successfully used to describe seed separation efficiency because in most practical applications, the error generated by the evaluated formulas did not exceed 1.5%.

Symbols

- a – share of crop seeds in a sample of purified seeds,
- a_p – share of crop seeds in the separated product,
- a_o – share of discarded crop seeds,
- b – share of impurities in a sample of purified seeds,
- b_i – share of impurities of the i^{th} species in a sample of purified seeds,
- b_p – share of impurities in the separated product,
- b_o – share of discarded impurities,
- b_{oi} – share of discarded impurities of the i^{th} species,
- c – purity of purified seeds,
- c_p – purity of the separated product,
- z – crop seed loss,
- ε_1 – crop seed yield,
- ε_2 – efficiency of impurity separation,
- ε_{2i} – efficiency of separating impurities of the i^{th} species,
- ε – efficiency of seed mixture separation.

* Correspondence: Zdzisław Kaliniewicz, Katedra Maszyn Roboczych i Metodologii Badań, Uniwersytet Warmińsko-Mazurski, ul. Oczapowskiego 11/B112, 10-719 Olsztyn, tel. +48 89 523-39-34, e-mail: zdzislaw.kaliniewicz@uwm.edu.pl

Introduction

In Poland, 75% of total crop acreage is dedicated to the production of cereal seeds. Other seed-producing plants include grasses, legumes, industrial crops, vegetables, culinary and medicinal herbs and ornamental plants. In addition to the main species, most field treatments contain other plant species which contaminate the main crop after harvest to a varied degree. Such impurities include the seeds of both crop plants and weeds (GROCHOWICZ 1994, PIETKIEWICZ, WIERZBICKI 1988, SEMCZYSZYN, FORNAL 1990). Seeds harvested from very clean and well-maintained treatments may contain organic (plant stems, leaves, husks, etc.) and mineral impurities (sand, gravel). In some cases, those impurities cannot be fully separated from crop seeds (SEMCZYSZYN, FORNAL 1990, RAWA, SEMCZYSZYN 1988, WIERZBICKI et al. 1991).

Seed mixtures have to be purified to meet qualitative requirements. Purification processes lead to a certain loss of crop seeds which are discarded together with impurities (CHOSZCZ, WIERZBICKI 1994, KALINIEWICZ 2011, GROCHOWICZ 1994, SEMCZYSZYN, FORNAL 1990). This does not pose a serious problems when weakly developed, broken or infected seeds are discarded. In many cases, separation leads to the elimination of healthy and plump seeds which are well suited for consumption or sowing (KALINIEWICZ et al. 1994, PIETKIEWICZ, WIERZBICKI 1988).

The results of the separation process can be described with the use of various indicators, such as product purity, crop seed yield, crop seed loss, separation efficiency of one or all types of impurities and efficiency of mixture separation. The latter concerns the entire seed mixture, and it should be the most comprehensive source of information for the user of a given separation device. The efficiency of seed mixture separation has been calculated by various authors with the use of two different formulas. The formulas could differ in their ability to accurately determine the efficiency of mixture separation.

The objective of this study was to evaluate the ability of two mathematical formulas to describe changes in seed purification parameters.

Theoretical assumptions

Indicators of seed separation quality can be determined based on the share (by number or weight) of different seed species in the mixture. The determination of the weight of every mix component and the calculation of the respective indices is an easier and a less time-consuming method. The number of separated seeds can be determined when purity standards for a given product define the maximum allowable number of contaminating seeds.

The purified mixture contains crop seeds as well as various impurities. Mixture purity can be determined with the use of the following formula:

$$c = \frac{a}{a + b} \quad (1)$$

As a result of separation, the first and second set are halved. One half is transferred to the separated product, and the other half is discarded. Therefore:

$$a = a_p + a_o \quad (2)$$

$$b = b_p + b_o \quad (3)$$

The separated product may be characterized by the following indicators:

– purity

$$c_p = \frac{a_p}{a_p + b_p} \quad (4)$$

– crop seed yield

$$\varepsilon_1 = \frac{a_p}{a} = \frac{a_p}{a_p + a_o} \quad (5)$$

– crop seed loss

$$z = 1 - \varepsilon_1 = \frac{a_o}{a_p + a_o} \quad (6)$$

The objective of the separation process is to eliminate impurities from raw material. The efficiency of separating a specific impurity is determined with the use of the following formula:

$$\varepsilon_{2i} = \frac{b_{oi}}{b_i} \quad (7)$$

and the efficiency of separating all impurities:

$$\varepsilon_2 = \frac{\sum b_{oi}}{\sum b_i} = \frac{b_o}{b} \quad (8)$$

For the separation process to be described by a single indicator, it has to account for both crop seed yield and the effectiveness of impurity separation. The following formula has been proposed by GROCHOWICZ (1994):

$$\varepsilon' = \varepsilon_1 - (1 - \varepsilon_2) \quad (9)$$

According to RAWA (1992, 1994), the efficiency of mixture separation can be determined with the use of the following formula:

$$\varepsilon'' = \varepsilon_1 \cdot \varepsilon_2 \quad (10)$$

The choice of the above formula was probably dictated by its widespread use, for example in calculations of the overall efficiency of technical devices (ADAMKIEWICZ, JARZECKI 2009, HETMAŃCZYK, WINCHULA 2012, KOJTYCH et al. 1998, KRAWCZYK 2010, KUCZEWSKI, MISZCZAK 1996, LISOWSKI, PANEK 2004, OSIŃSKI 2012, SZULC, KOCZARA 2005). To date, the information content and the ability of formulas (9) and (10) to determine the efficiency of mixture separation has not been compared in literature.

Experimental design

The experiment was designed for a hypothetical mixture of seeds containing 90% crop seeds and 10% seeds of contaminating plant species. The following change scenarios were analyzed to determine correlations between indicators of the separation process:

a) variant I – the share of crop seeds in the separated product increases (from 0.4 to 0.9) with an increase in the share of discarded impurities (from 0 to 0.1),

b) variant II – the share of crop seeds in the separated product is constant (0.8) and the share of discarded impurities increases (from 0 to 0.1),

c) variant III – the share of crop seeds in the separated product increases (from 0.4 to 0.9) and the share of discarded impurities is constant (0.07),

d) variant IV – the share of crop seeds in the separated product decreases (from 0.9 to 0.4) and the share of discarded impurities increases (from 0 to 0.1),

e) variant V – the share of crop seeds in the separated product decreases (from 0.9 to 0.1) proportionally to an increase in the share of discarded impurities (from 0 to 0.1).

Results and Discussion

The simulated separation values of a hypothetical seed mixture were presented in Tables 1 to 5. In the analyzed variants, the purity of the separated product ranged from 80% to 100%. The above indicated that case scenarios with highly unfavorable and incorrect separation parameters were also analyzed because the separated product was characterized by lower purity than the raw material. The classification of the separated fractions should be reversed, and if the resulting seed loss were excessive, a given separation process should be abandoned.

Table 1

Indicators of seed mixture separation efficiency – variant I

a_p [-]	a_o [-]	b_p [-]	b_o [-]	c_p [-]	ε_1 [-]	ε_2 [-]	ε' [-]	ε'' [-]
0.40	0.50	0.10	0	0.800	0.444	0	-0.556	0
0.45	0.45	0.09	0.01	0.833	0.500	0.100	-0.400	0.050
0.50	0.40	0.08	0.02	0.862	0.556	0.200	-0.244	0.111
0.55	0.35	0.07	0.03	0.887	0.611	0.300	-0.089	0.183
0.60	0.30	0.06	0.04	0.909	0.667	0.400	0.067	0.267
0.65	0.25	0.05	0.05	0.929	0.722	0.500	0.222	0.361
0.70	0.20	0.04	0.06	0.946	0.778	0.600	0.378	0.467
0.75	0.15	0.03	0.07	0.962	0.833	0.700	0.533	0.583
0.80	0.10	0.02	0.08	0.976	0.889	0.800	0.689	0.711
0.85	0.05	0.01	0.09	0.988	0.944	0.900	0.844	0.850
0.90	0	0	0.10	1	1	1	1	1

Source: own calculations.

Table 2

Indicators of seed mixture separation efficiency – variant II

a_p [-]	a_o [-]	b_p [-]	b_o [-]	c_p [-]	ε_1 [-]	ε_2 [-]	ε' [-]	ε'' [-]
0.80	0.10	0.10	0	0.889	0.889	0	-0.111	0
		0.09	0.01	0.899	0.889	0.100	-0.011	0.089
		0.08	0.02	0.909	0.889	0.200	0.089	0.178
		0.07	0.03	0.920	0.889	0.300	0.189	0.267
		0.06	0.04	0.930	0.889	0.400	0.289	0.356
		0.05	0.05	0.941	0.889	0.500	0.389	0.444
		0.04	0.06	0.952	0.889	0.600	0.489	0.533
		0.03	0.07	0.964	0.889	0.700	0.589	0.622
		0.02	0.08	0.976	0.889	0.800	0.689	0.711
		0.01	0.09	0.988	0.889	0.900	0.789	0.800
		0	0.10	1	0.889	1	0.889	0.889

Source: own calculations.

Table 3

Indicators of seed mixture separation efficiency – variant III

a_p [-]	a_o [-]	b_p [-]	b_o [-]	c_p [-]	ε_1 [-]	ε_2 [-]	ε' [-]	ε'' [-]
0.40	0.50			0.930	0.444		0.144	0.311
0.45	0.45			0.938	0.500		0.200	0.350
0.50	0.40			0.943	0.556		0.256	0.389
0.55	0.35			0.948	0.611		0.311	0.428
0.60	0.30			0.952	0.667		0.367	0.467
0.65	0.25	0.03	0.07	0.956	0.722	0.700	0.422	0.506
0.70	0.20			0.959	0.778		0.478	0.544
0.75	0.15			0.962	0.833		0.533	0.583
0.80	0.10			0.964	0.889		0.589	0.622
0.85	0.05			0.966	0.944		0.644	0.661
0.90	0			0.968	1		0.700	0.700

Source: own calculations.

Table 4

Indicators of seed mixture separation efficiency – variant IV

a_p [-]	a_o [-]	b_p [-]	b_o [-]	c_p [-]	ε_1 [-]	ε_2 [-]	ε' [-]	ε'' [-]
0.90	0	0.10	0	0.900	1	0	0	0
0.85	0.05	0.09	0.01	0.904	0.944	0.100	0.044	0.094
0.80	0.10	0.08	0.02	0.909	0.889	0.200	0.089	0.178
0.75	0.15	0.07	0.03	0.915	0.833	0.300	0.133	0.250
0.70	0.20	0.06	0.04	0.921	0.778	0.400	0.178	0.311
0.65	0.25	0.05	0.05	0.929	0.722	0.500	0.222	0.361
0.60	0.30	0.04	0.06	0.938	0.667	0.600	0.267	0.400
0.55	0.35	0.03	0.07	0.948	0.611	0.700	0.311	0.428
0.50	0.40	0.02	0.08	0.962	0.556	0.800	0.356	0.444
0.45	0.45	0.01	0.09	0.978	0.500	0.900	0.400	0.450
0.40	0.50	0	0.10	1	0.444	1	0.444	0.444

Source: own calculations.

Table 5

Indicators of seed mixture separation efficiency – variant V

a_p [-]	a_o [-]	b_p [-]	b_o [-]	c_p [-]	ε_1 [-]	ε_2 [-]	ε' [-]	ε'' [-]
0.90	0	0.10	0	0.900	1	0	0	0
0.82	0.08	0.09	0.01	0.901	0.911	0.100	0.011	0.091
0.74	0.16	0.08	0.02	0.902	0.822	0.200	0.022	0.164
0.66	0.24	0.07	0.03	0.904	0.733	0.300	0.033	0.220
0.58	0.32	0.06	0.04	0.906	0.644	0.400	0.044	0.258
0.50	0.40	0.05	0.05	0.909	0.556	0.500	0.056	0.278
0.42	0.48	0.04	0.06	0.913	0.467	0.600	0.067	0.280
0.34	0.56	0.03	0.07	0.919	0.378	0.700	0.078	0.264
0.26	0.64	0.02	0.08	0.929	0.289	0.800	0.089	0.231
0.18	0.72	0.01	0.09	0.947	0.200	0.900	0.100	0.180
0.10	0.80	0	0.10	1	0.111	1	0.111	0.111

Source: own calculations.

The efficiency of mixture separation calculated from formula (10) is equal to zero or is higher than zero, whereas separation efficiency determined based on formula (9) takes on both positive and negative values. Negative values were obtained in separation variants where the purity of the separated product deteriorated. In this case, the separation process is reversed. Owing to the number of discarded crop seeds, discarded material was characterized by higher purity than the material accumulated in the main container of a hypothetical separation device.

The discussed indicators had identical values when crop seed yield or the efficiency of impurity separation or both indicators were equal to 1. The efficiency of mixture separation calculated based on formula (9) was lower than that determined with the use of formula (10).

When both indicators of mixture separation efficiency were higher than 0.5, the resulting difference in indicator values did not exceed 12.5% (Fig. 1). Under relatively satisfactory separation conditions (crop seed loss of up to 10% and efficiency of impurity separation higher than 80%), the maximum difference between indicators of separation efficiency calculated with both formulas is 0.02, and the resulting error did not exceed 3%. Both formulas can be used to determine the analyzed indicator when crop seed yield and the efficiency of impurity separation are high because in most practical applications (CHOSZCZ, WIERZBICKI 1994, PIETKIEWICZ, WIERZBICKI 1988, RAWA 1992, 1994, SEMCZYŹYŃ, FORNAL 1990), the value of the separation efficiency indicator is higher than 0.8.

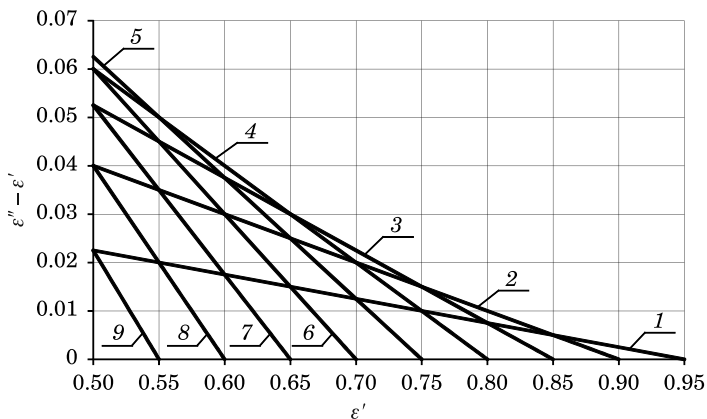


Fig. 1. Differences in the values of indicators of seed mixture separation efficiency calculated with the use of two mathematical formulas for crop seed yield of: 1 – 0.95, 2 – 0.90, 3 – 0.85, 4 – 0.80, 5 – 0.75, 6 – 0.70, 7 – 0.65, 8 – 0.60, 9 – 0.55

Source: own study.

Conclusions

1. A mathematical formula determining the efficiency of mixture separation, construed as the difference between crop seed yield and the share of impurities in the separated product, takes on both positive and negative values. Negative values indicate that the separation process has been reversed.

2. A mathematical formula for determining the efficiency of mixture separation, construed as a product of crop seed yield and the efficiency of impurity separation, always takes on positive values regardless of whether the separation process has been reversed.

3. The difference in determinations of separation efficiency (the minimum value of the indicator of separation efficiency is 0.5) performed with the use of both mathematical formulas is maximum 8%, and it decreases with an improvement in separation quality.

4. Both mathematical formulas can be applied to evaluate separation processes because in most practical applications, the minimum value of the indicator of separation efficiency is 0.8 and the resulting error does not exceed 1.5%.

Translated by ALEKSANDRA POPRAWKA

References

- ADAMKIEWICZ A., JARZEŃKI Ł. 2009. *Comparative analysis of operational properties of propulsion systems of RoPax type ships*. Eksploatacja i Niezawodność, 2: 52–62.
- CHOSZCZ D., WIERZBICKI K. 1994. *An analysis of the efficiency of currently applied processing lines for winnowing rape and mustard seeds in separating field bedstraw (Galium aparine) seeds*. Acta Acad. Agricult. Techn. Ols., Aedif. Mech., 25: 71–80.
- GROCHOWICZ J. 1994. *Maszyny do czyszczenia i sortowania nasion*. Wyd. AR, Lublin.
- HETMAŃCZYK I., WINCHULA Ł. 2012. *Hybrid drive for agricultural vehicles*. Inżynieria Rolnicza, 2(137): 77–88.
- KALINIEWICZ Z. 2011. *The effect of the impurity content of buckwheat nutlets on product purity after cleaning in a grader with indented pockets*. Technical Sciences, 14: 5–12.
- KALINIEWICZ Z., KONOPKA S., RAWA T. 1994. *Problems of the buckwheat grain cleaning*. Materiały III Ogólnopolskiej i II Międzynarodowej Konferencji Naukowej „Rozwój teorii i technologii w technicznej modernizacji rolnictwa”, Olsztyn: 252–256.
- KOJTYCH A., SZAWŁOWSKI M., SZYMCZYK W. 1998. *Pracownia techniczna*. 1. Wyd. WSiP, Warszawa.
- KRAWCZYK D. 2010. *The basic factors influencing energy consumption in offices*. Budownictwo i Inżynieria Środowiska, 1: 137–142.
- KUCZEWSKI J., MISZCZAK M. 1996. *Podstawy konstrukcji maszyn rolniczych i leśnych*. Wyd. SGGW, Warszawa.
- LISOWSKI E., PANEK M. 2004. *CFD modeling of vane pump vanes operation*. Eksploatacja i Niezawodność, 2: 36–41.
- OSIŃSKI Z. 2012. *Podstawy konstrukcji maszyn*. Wydawnictwo Naukowe PWN, Warszawa.
- PIETKIEWICZ T., WIERZBICKI K. 1988. *Analysis of efficiency of rape seeds winnowing in the state corn plants*. Acta Acad. Agricult. Techn. Ols., Aedif. Mech., 18: 111–119.
- RAWA T. 1992. *A study of the buckwheat grain clearing effectiveness*. Acta Acad. Agricult. Techn. Ols., Aedif. Mech., 22, Supplementum A.

-
- RAWA T. 1994. *An analysis of the efficiency of buckwheat seeds winnowing in a trieur*. Acta Acad. Agricult. Techn. Ols., Aedif. Mech., 25: 81–87.
- RAWA T., SEMCZYSZYN M. 1988. *Analysis of methods of qualifying of grain compositions distribution in winnowing problems*. Acta Acad. Agricult. Techn. Ols., Aedif. Mech., 18: 41–53.
- SEMCZYSZYN M., FORMAL Ł. 1990. *Analysis of work effectiveness of winnowing devices used in the process lines of buckwheat grain winnowing. II. Results of examination of work quality of winnowing devices*. Acta Acad. Agricult. Techn. Ols., Aedif. Mech., 21: 111–121.
- SZULC Z., KOCZARA W. 2005. *Improving energy efficient of drive system with medium voltage induction motor by using frequency converter*. Zeszyty Problemowe – Maszyny Elektryczne, 73: 49–53.
- WIERZBICKI K., PIETKIEWICZ T., CHOSZCZ D., MAŃKOWSKI S. 1991. *Effectiveness of the wheat grain cleaning process with complex movement of sieve basket*. Acta Acad. Agricult. Techn. Ols., Aedif. Mech., 22: 179–189.

STRING SIEVE: DESIGN CONCEPT AND PARAMETERS

Zdzisław Kaliniewicz

Department of Heavy Duty Machines and Research Methodology
University of Warmia and Mazury, Poland

Received 8 March 2013; Accepted 17 May 2013; Available on line 15 July 2013

Key words: seed cleaning and sorting, geometric parameters, string sieve.

Abstract

This paper presents the design concept and the parameters of a new device for cleaning and-or sorting seeds and grain produced in a conventional farm. The discussed device is a string sieve where the groove between adjacent strings is minimal at the beginning of the screen and increases towards the end of the screen. The proposed sieve poses an alternative to a screen separator comprising a set of differently-sized mesh screens with longitudinal openings. In view of the average size of farm-produced seeds, the width of the separating groove should be set at 1 mm at the beginning of the screen and 11 mm at the end of the screen. In sieves not designed for grading large seeds or vetch seeds, the width of the separating groove can be set at 1 mm and 5 mm, respectively.

Symbols:

- d_s – string diameter,
- L – screen length,
- r_s – string spacing,
- s – width of groove at distance x from the beginning of the screen,
- s_k – width of separating groove at the end of the screen,
- s_p – width of separating groove at the beginning of the screen,
- s_{s1} – maximum width of the groove between the top string and the bottom string in the first row,
- s_{s2} – maximum width of the groove between the top string and the bottom string in the second row,
- x – distance from the beginning of the screen,
- β_1 – angle of inclination of bottom strings in the first row relative to top strings,
- β_2 – angle of inclination of bottom strings in the second row relative to top strings,
- γ – opening angle between strings in bottom rows.

* Correspondence: Zdzisław Kaliniewicz, Katedra Maszyn Roboczych i Metodologii Badań, Uniwersytet Warmińsko-Mazurski, ul. Oczapowskiego 11/B112, 10-719 Olsztyn, tel. +48 89 523-39-34, e-mail: zdzislaw.kaliniewicz@uwm.edu.pl

Introduction

A screen separator containing ten or more screens with different mesh sizes is one of the most popular devices for cleaning and sorting seeds. A screen separator comprises mesh screens with longitudinal and round openings whose dimensions are determined by the separator's grading efficiency and seed species. Mesh openings have regular shape and size across the entire screen. A single mesh screen can be applied to separate seeds into two fractions only: seeds that are captured by the mesh and seeds that pass through the mesh (GROCHOWICZ 1994). A seed mixture is separated by a mesh screen when the size of mesh openings falls within the distribution range of a given physical attribute of seeds, such as thickness or width. Several mesh screens are placed in the separator bucket to separate seeds into more than two fractions. Different screens are used to separate various seed species or differently sized seeds of the same species. Due to the fact that the above process is laborious and time-consuming, efforts were undertaken to develop a new solution for a cleaning machine that would not require mechanical modification to separate seeds of different species.

A string sieve for cleaning and sorting seeds has been developed by the author (KALINIEWICZ 2011). This paper analyzes the structure and geometric parameters of a string sieve, and it examines the proposed device's ability to clean and sort the principal seed species produced by a conventional farm.

Structure of a string sieve

A string sieve was designed as an alternative for a conventional screen separator containing a set of exchangeable mesh screens with longitudinal openings. The proposed sieve will be used for sorting and cleaning seeds produced by a conventional farm. The designed sorting device with a single separating element is easy to operate and control.

The operating element in the proposed sorting machine is a surface with grooves whose width is minimal at the beginning of the screen and increases towards the end of the screen. The screen is set at a certain angle, and the seed mixture which is fed at the beginning of the screen slides down the screen automatically or when it is set into reciprocating motion. The seed mixture travels across the screen, and increasingly thicker fractions are separated as seeds move away from the beginning of the screen (feeding point). The operating element does not contain flat surfaces which would allow the seeds to bypass the respective separation areas.

A structural diagram of a string sieve (KALINIEWICZ 2011) is presented in Figure 1. Strings are stretched between two horizontal bars. At the beginning of the screen, strings are separated by equal distances in a single row (with

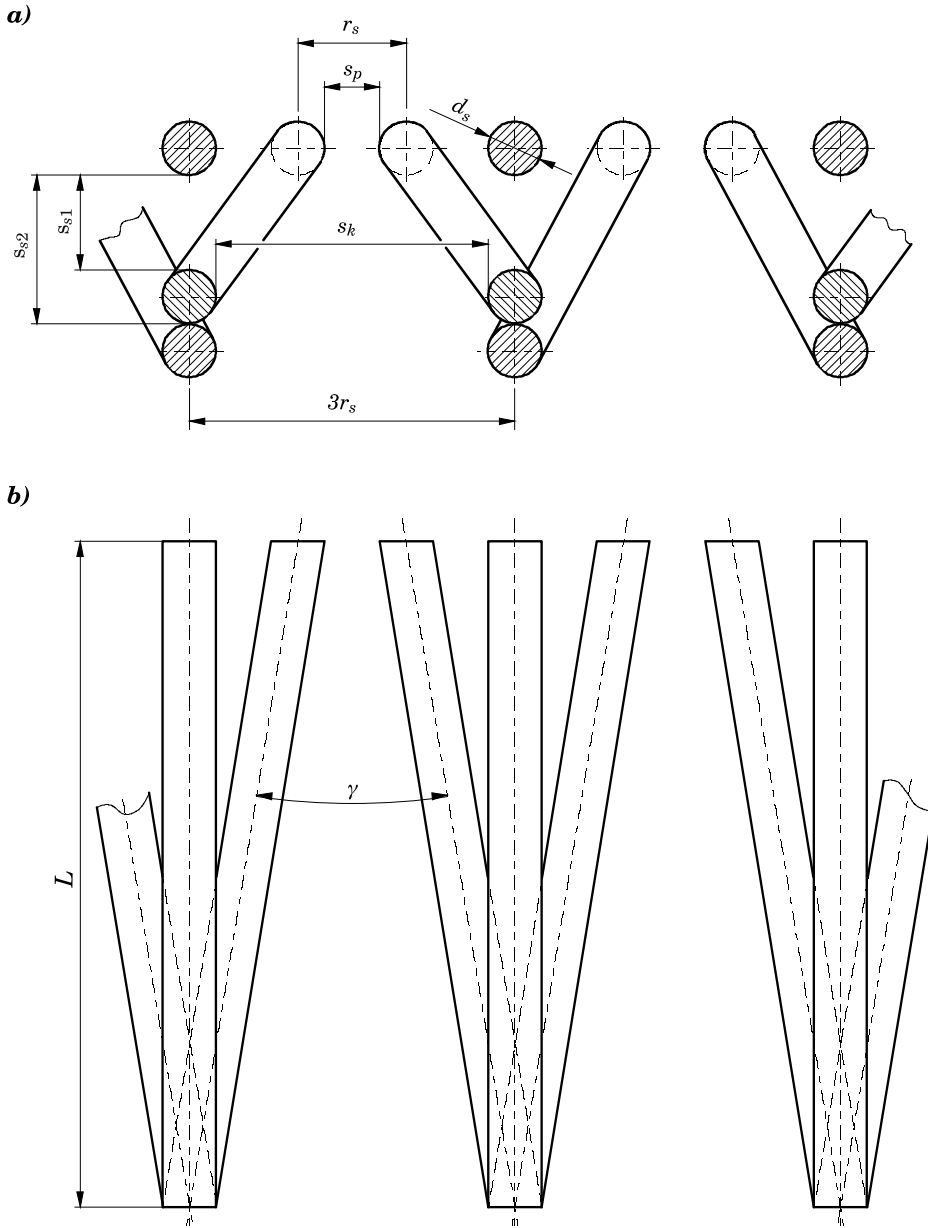


Fig. 1. String arrangement in a string sieve: *a* – rear view, *b* – top view

string spacing r_s), and the width of openings s_p between strings has to be smaller than the thickness of the finest seeds of the principal species. At the end of the screen, strings are stretched in three rows, and every set of three strings is set in a vertical plane (one string under another). The width of the opening s_k between strings should be larger than the thickness of the largest seeds of the principal species. This arrangement creates a separating groove along the screen, and its size changes gradually with distance from the beginning of the screen in the range of s_p to s_k . Lateral grooves are formed between top and bottom row strings, and their width changes along the screen in the range of s_p to s_{s1} or s_{s2} . Seeds are not sorted by lateral grooves whose width is identical to that of the separating groove only at the beginning of the screen and continues to decrease towards the end of the screen. Seeds which initially fall into lateral grooves due to the designed string arrangement will move perpendicularly to the angle of inclination of lateral grooves, and they will ultimately fall into the main separating grooves. Seeds are sorted into various size fractions by changing the position of collecting buckets under the screen.

A string sieve can be made of wires or rods with circular, square, triangular or hexagonal cross-section. Strings with non-circular cross-section have to be turned around their axis to ensure that their flat surface is not aligned perpendicularly to screen surface. Strings can be made of various materials with the required strength, and they may be additionally coated with rubber or plastic. A sieve comprising strings with a circular cross-section will be analyzed in this paper.

The width of the separating groove at the beginning and end of the screen can be determined with the use of the following formulas:

$$s_p = r_s - d_s \quad (1)$$

$$s_k = 3r_s - d_s \quad (2)$$

and the resulting values are transformed to produce:

$$d_s = \frac{s_k - 3s_p}{2} \quad (3)$$

$$r_s = \frac{s_k - s_p}{2} \quad (4)$$

Thus, the specific widths of the separating groove at the beginning and end of the screen correspond to a single arrangement of string spacing and string diameter. The width of the separating groove changes with distance from the beginning of the screen. In line with the principle of similar triangles (Fig. 2):

$$\frac{(s - s_p)}{x} = \frac{(s_k - s_p)}{L} \quad (5)$$

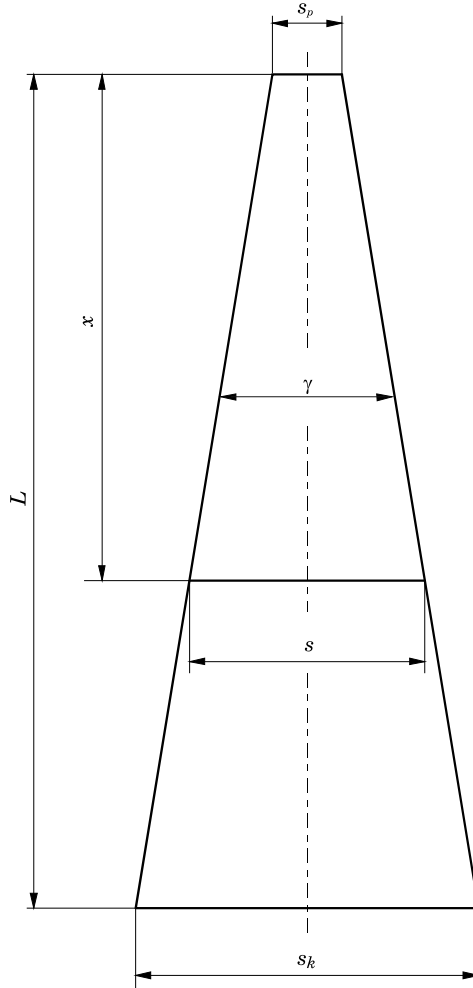


Fig. 2. Groove parameters in a string sieve

When formula (5) is transformed accordingly, the width of groove s at a given point in the screen is described by the following dependency:

$$s = \frac{(s_k - s_p) \cdot x}{L} + s_p \quad (6)$$

At this point, seeds whose thickness matches the width of the groove should be placed in the collection bucket, while larger seeds should travel further across the surface of the sieve.

Based on general trigonometric equations, the opening angle between strings γ can be determined from the following formula:

$$\gamma = \arctg \frac{s_k - s_p}{L} \quad (7)$$

and the angle of inclination between top and bottom strings:

$$\beta_1 = \arctg \frac{s_{s1} + d_s}{L} \quad (8)$$

$$\beta_2 = \arctg \frac{s_{s2} + d_s}{L} \quad (9)$$

In principle, lateral grooves between top and bottom strings (s_{s1} and s_{s2} at the end of the screen) (Fig. 1) are not designed for seed grading. To prevent seeds from leaving the screen via lateral grooves, the width of lateral grooves should not exceed the width of the main separating groove s_k . Since bottom row strings at the end of the screen form two levels, the above requirement applies mainly to the width of groove s_{s2} because in accordance with the below formula, the width of groove s_{s1} is always smaller:

$$s_{s2} = s_{s1} + d_s \quad (10)$$

Based on the assumption that grooves have equal width, i.e. $s_{s2} = s_k$, and in view of equation (3), equations (8) and (9) take on the following form:

$$\beta_1 = \arctg \frac{s_k}{L} \quad (11)$$

$$\beta_2 = \arctg \frac{3(s_k - s_p)}{2L} \quad (12)$$

The proposed arrangement of strings, which results in the above angles between strings, increases grading efficiency because seeds move across the surface of the sieve faster than implied by its angle of inclination.

Geometric attributes of seeds

Seed cleaning and grading machines have to be designed in view of the physical parameters of processed material (GROCHOWICZ 1994). Physical attributes are needed to design successive stages of the separation process and produce seed material of required quality (MAJEWSKA et al. 2000). A knowledge of the processed material's physical parameters is also required to model production, acquisition, transportation, cleaning, sorting, drying and storage processes (ALTUNTAS, DEMIRTOLA 2007, ÇALIŞIR et al. 2005, DAVIES, EL-OKENE 2009, GROCHOWICZ 1994, KALKAN, KARA 2011, KUSIŃSKA 2004, RYBIŃSKI, SZOT 2009).

Seed dimensions are determined by various factors, mostly soil and climate conditions, agricultural practices and the varietal characteristics of seeds (*Szczegółowa...* 2003a, 2003b). Variations in seed size may also result from seed position on the maternal plant (BRZEZIŃSKI, KLOCKIEWICZ-KAMIŃSKA 1997, FORMAL, KUBIAK 1995, GEODECKI, GRUNDAS 2003), seed moisture content (ALTUNTAS, DEMIRTOLA 2007, ÇALIŞIR et al. 2005, DAVIES, EL-OKENE 2009, GHARIBZAHEDI et al. 2011, IZLI et al. 2009, KALKAN, KARA 2011, KUSIŃSKA 2004, KUSIŃSKA et al. 2010, SOLOGUBIK et al. 2013, YALÇIN et al. 2007) and time of storage (KUSIŃSKA 2004).

A knowledge of the basic geometric parameters of separated seeds, in particular seed thickness, is required for the proposed device to pose an effective alternative to a screen separator containing a set of mesh screens with longitudinal openings.

The dimensions of various seed species with adequate storage moisture levels, without an indication of seed cultivar or cultivation method, are presented in Table 1. The thickness of fine seeds (rapeseed, mustard) varies in the range of 1.1 to 2.5 mm. The thickness of principal cereal seeds ranges from 1.2 mm (oats and rye) to 4.7 mm (barley). Similar values are reported for buckwheat seeds, whereas vetch seeds may be somewhat larger (up to 6.1 mm). The thickness of larger grain seeds varies in the range of 2.9 mm (lupine) to 10.1 mm (pea). As shown by Table 1 data, seeds produced by a typical agricultural farm can be classified into the following size ranges:

- thickness – 1.1 ÷ 10.1 mm,
- width – 1.1 ÷ 10.8 mm,
- length – 1.4 ÷ 18.6 mm.

Table 1

Geometric parameters of seeds

Seed species	Seed group	Dimensions			References
		thickness [mm]	width [mm]	length [mm]	
Mustard Rapeseed	I	1.1÷2.4	1.1÷2.7	1.4÷3.0	3, 4
		1.2÷2.5	1.6÷2.8	1.7÷2.8	1, 4, 24, 25, 26
Barley	II	1.4÷4.7	2.0÷5.0	7.0÷14.6	6, 11, 12, 13
Oats		1.2÷3.6	1.4÷4.0	8.0÷18.6	6, 11, 18
Wheat		1.4÷3.9	1.6÷4.5	4.3÷10.2	6, 19, 20, 21, 22, 23
Triticale		1.7÷4.1	1.9÷4.3	5.3÷10.4	1, 21
Rye		1.2÷3.5	1.5÷3.6	5.0÷10.5	21, 27, 28
Buckwheat		2.0÷4.2	3.0÷5.2	4.4÷8.0	6, 9, 10
Vetch	III	2.0÷6.1	3.2÷6.3	3.2÷7.5	1, 6, 7
Faba bean	IV	5.5÷9.9	5.8÷10.8	7.1÷14.2	1, 2
Pea		3.5÷10.1	3.7÷10.2	4.0÷10.5	5, 6, 7, 8
Lupine		2.9÷8.5	3.1÷8.5	3.9÷13.6	6, 14, 15, 16, 17

1 – MARKOWSKI (2007), 2 – MIESZKALSKI (1991), 3 – JADWISIEŃCZAK, KALINIEWICZ (2011), 4 – CHOSZCZ, WIERZBICKI (1994), 5 – ALTUNTAS, DEMIRTOLA (2007), 6 – GROCHOWICZ (1994), 7 – RYBIŃSKI et al. (2009), 8 – YALÇIN et al. (2007), 9 – KALINIEWICZ, RAWA (2001), 10 – KRAM et al. (2007), 11 – HEBDA, MICEK (2007), 12 – SADOWSKA, ŻABIŃSKI (2009), 13 – SOLOGUBIK et al. (2013), 14 – KAMIŃSKA, ANDREJKO (2006), 15 – LEMA et al. (2005), 16 – MAŃKOWSKI (2004), 17 – SADOWSKA, ŻABIŃSKI (2011), 18 – KUSIŃSKA (2004), 19 – CHOSZCZ et al. (2010), 20 – GEODECKI, GRUNDAS (2003), 21 – HEBDA, MICEK (2005), 22 – KALKAN, KARA (2011), 23 – SEGIT et al. (2003), 24 – ÇALIŞIR et al. (2005), 25 – IZLI et al. (2009), 26 – RAWA et al. (1990), 27 – KUSIŃSKA et al. (2010), 28 – ZDYBEL et al. (2009).

Parameters of a string sieve

In accordance with Equations (3) and (4), the specific widths of the separating groove at the beginning and end of the screen correspond to a single arrangement of string spacing and string diameter. The parameters of a sieve for grading various seed species are presented in Table 2. According to the methodological assumptions, the surface of the string sieve should be used in the sorting process to the highest possible degree, i.e. the width of a given groove at the beginning of the screen should be somewhat smaller than the thickness of the finest seeds of the principle species, and the width of the groove at the end of the screen – somewhat larger than the thickness of the largest seeds of the principal species. The width of the groove for separating fine seeds (group I) should be 1 mm at the beginning of the screen and 3 mm at the end of the screen. In line with formula (3), a string sieve cannot be designed for the above parameters because string thickness $d_s = 0$ mm. If string thickness $d_s = 0.5$ mm and if the width of the groove at the beginning of the screen $s_p = 1$ mm, then based on formula (3), the width of the groove at the end of the screen $s_k = 4$ mm. In this situation, the screen will not be fully utilized

Table 2
Parameters of a string sieve for grading groups of seeds of different thickness

Parameter	Seed group						
	I	II	I+II	III	I+II+III	IV	I+II+III+IV
s_p [mm]	1.0	1.0	1.0	1.5	1.0	2.5	1.0
s_k [mm]	(3.0) 4.0	5.0	5.0	6.5	6.5	11.0	11.0
d_s [mm]	(0) 0.5	1.0	1.0	1.0	1.75	1.75	4.0
r_s [mm]	(1.0) 1.5	2.0	2.0	2.5	2.75	4.25	5.0

I – fine seeds (rapeseed, mustard),

II – principal cereals (wheat, rye, barley, oats and triticale) and buckwheat,

III – vetch,

IV – large seeds (pea, lupine, faba bean).

because all seeds will fall through the grooves at approximately 2/3 of its length.

For cereal and buckwheat seeds (group II), the width of the groove at the beginning and end of the screen should be 1 mm and 5 mm, respectively, with string diameter of 1 mm and string spacing of 2 mm. A sieve with string diameter of 1 mm and string spacing of 2.5 mm can be applied to sort vetch seeds (group III) because the resulting width of the grooves at the beginning and end of the screen will reach 1.5 mm and 6.5 mm, respectively. A sieve for grading seeds from groups I, II and III should comprise strings with the diameter of 1.75 mm, separated by a distance of 2.75 mm. The resulting width of the groove would reach 1 mm at the beginning of the screen and 6.5 mm at the end of the screen. A sieve for sorting larger seeds (group IV) should be designed with groove width of 2.5 mm and 11 mm at the beginning and end of the screen, respectively. This solution requires strings with the diameter of 1.75 mm and string spacing of 4.25 mm.

In a sieve capable of separating all of the seed species given in Table 1 (groups I, II, III and IV), the width of the separating groove should be set at 1 mm at the beginning of the screen and at 11 mm at the end of the screen. In sieves designed for grading principal cereal seeds, buckwheat seeds and fine seeds (groups I and II), the respective parameters should be 1 mm and 5 mm.

The proposed string sieve will sort seeds into minimum three size fractions, and the sorting surface for each fraction will have the minimum length of 20 cm. This means that total sieve length will be minimum $L = 60$ cm. If the separating groove at the end of the screen has the width $s_k = 11$ mm, the opening angle between strings will reach $\gamma = 0.95^\circ$. Sieves which are longer and/or have narrower grooves at the end of the screen will have a smaller opening angle between strings.

In a sieve with minimum length ($L = 60$ cm) and the widest groove at the end of the screen ($s_k = 11$ mm), the angles of inclination of bottom strings relative to top strings will reach $\beta_1 = 1.05^\circ$ and $\beta_2 = 1.43^\circ$, respectively. Sieves which are longer and/or have narrower grooves at the end of the screen will have smaller angles of inclination.

Conclusions

The proposed string sieve poses an alternative for a screen separator comprising a set of mesh screens with longitudinal openings. The width of separating grooves changes gradually towards the end of the screen. In the designed sieve, seeds are separated into different fractions by changing the position of collection buckets under the string sieve. In devices capable of separating the majority of seeds produced by a conventional farm, the width of the separating groove should be set at 1 mm at the beginning of the screen and at 11 mm at the end of the screen. In sieves which are not designed for grading large seeds (faba bean, pea, lupine) or vetch seeds, the respective parameters should be 1 mm and 5 mm.

Translated by ALEKSANDRA POPRAWKA

References

- ALTUNTAS E., DEMIRTOLA H. 2007. *Effect of moisture content on physical properties of some grain legume seeds*. New Zealand Journal of Crop and Horticultural Science, 35: 423–433.
- BRZEZIŃSKI W.J., KLOCKIEWICZ-KAMIŃSKA E. 1997. *Produkcja mąki wypiekowej w Polsce – utopia czy rzeczywistość w zasięgu ręki?* Przegląd Zbożowo-Młynarski, 8: 15–18.
- ÇALISIR S., MARAKOĞLU T., ÖĞÜT H., ÖZTÜRK Ö. 2005. *Physical properties of rapeseed (Brassica napus oleifera L.)*. Journal of Food Engineering, 69: 61–66.
- CHOSZCZ D., KONOPKA S., ZALEWSKA K. 2010. *Characteristics of physical properties of selected varieties of spelt*. Inżynieria Rolnicza, 4(122): 23–28.
- CHOSZCZ D., WIERZBICKI K. 1994. *A study the separation of field bedstraw (Galium aparine) seeds from rape and mustard seeds with the use of their geometrical and aerodynamic properties*. Acta Acad. Agricult. Tech. Olst. Aedif. Mech., 25: 61–69.
- DAVIES R.M., EL-OKENE A.M. 2009. *Moisture-dependent physical properties of soybeans*. Int. Agrophysics, 23: 299–303.
- FORNAL Ł., KUBIAK A. 1995. *Wykorzystanie komputerowej analizy obrazu do pomiaru cech geometrycznych i oceny wyrównania ziarna pszenicy*. Przegląd Zbożowo-Młynarski, 39(6): 22–25.
- GEODECKI M., GRUNDAS S. 2003. *Characterization of geometrical features of single Winter and spring wheat kernels*. Acta Agrophysica, 2(3): 531–538.
- GHARIBZAHEDI S.M.T., MOUSAVI S.M., GHAHDERJANI M. 2011. *A survey on moisture-dependent physical properties of castor seed (Ricinus communis L.)*. AJCS – Australian Journal of Crop Science, 5(1): 1–7.
- GROCHOWICZ J. 1994. *Maszyny do czyszczenia i sortowania nasion*. Wyd. Akademii Rolniczej, Lublin.
- HEBDA T., MICEK P. 2005. *Dependences between geometrical features of cereal grain*. Inżynieria Rolnicza, 6: 233–241.

- HEBDA T., MICEK P. 2007. *Geometric features of grain for selected corn varieties*. Inżynieria Rolnicza, 5(93): 187–193.
- IZLI N., UNAL H., SINCİK M. 2009. *Physical and mechanical properties of rapeseed at different moisture content*. Int. Agrophysics, 23: 137–145.
- JADWISIEŃCZAK K., KALINIEWICZ Z. 2011. *Analysis of the mustard seeds cleaning process*. Part 1. *Physical properties of seeds*. Inżynieria Rolnicza, 9(134): 57–64.
- KALINIEWICZ Z. 2011. *Sito strunowe*. Zgłoszenie patentowe nr P.396745, 24.10.2011.
- KALINIEWICZ Z., RAWA T. 2001. *Analysis of geometrical characteristics of buckwheat seeds with respect to determining shape and dimensions of cylindrical trieurs pits*. Problemy Inżynierii Rolniczej, 1: 21–28.
- KALKAN F., KARA M. 2011. *Handling, frictional and technological properties of wheat as affected by moisture content and cultivar*. Powder Technology, 213: 116–122.
- KAMIŃSKA A., ANDREJKO D. 2006. *Application of an analysis of main components in a research of the influence of moistening of yellow lupin seeds of Radames variety on their size*. Inżynieria Rolnicza, 7: 241–246.
- KRAM B.B., WOLIŃSKI J., WOLIŃSKA A. 2007. *Comparative studies on geometric traits of nutlets with and without seed cover in Red corolla buckwheat*. Acta Agrophysica, 9(3): 657–664.
- KUSIŃSKA E. 2004. *The influence of storage time, moisture content and self-warming up on selected geometrical parameters of oat grain*. MOTROL – Motoryzacja i Energetyka Rolnictwa, 6: 146–153.
- KUSIŃSKA E., KOBUS Z., NADULSKI R. 2010. *Impact of humidity on physical and geometrical properties of Slavic varieties of rye grains*. Inżynieria Rolnicza, 4(122): 151–156.
- LEMA M., SANTALLA M., RODIÑO A.P., DE RON A.M. 2005. *Field performance of natural narrow-leafed lupin from the northwestern Spain*. Euphytica, 144: 341–351.
- MAJEWSKA K., GUDACZEWSKI W., FORNAL Ł. 2000. *The size of wheat kernels and the rheological properties of dough*. Inżynieria Rolnicza, 5(16): 153–162.
- MAŃKOWSKI S. 2004. *Metoda rozdrabniania nasion lubinu i wydzielania cząstek okrywy nasiennej*. Rozprawa doktorska, Wydział Nauk Technicznych, UWM Olsztyn.
- MARKOWSKI P. 2007. *Analiza równomierności dozowania nasion koleczkowymi zespołami wysiewającymi*. Rozprawa doktorska, Wydział Nauk Technicznych, UWM Olsztyn.
- MIESZKALSKI L. 1991. *Influence of moisture on the geometrical features of faba bean seeds and also variation of these features with given variety*. Acta Acad. Agricult. Tech. Olst. Aedif. Mech., 22: 43–55.
- RAWA T., WIERZBICKI K., PIETKIEWICZ T. 1990. *Potential effectiveness of rape seeds cleaning according to geometrical characteristics*. Acta Acad. Agricult. Tech. Olst. Aedif. Mech., 20: 117–129.
- RYBIŃSKI W., SZOT B. 2009. *Relations between agrophysics and genetic and breeding of cereals and legumes*. Acta Agrophysica, Rozprawy i monografie, 174. Wyd. Instytut Agrofizyki im. Bohdana Dobrzańskiego PAN, Lublin.
- RYBIŃSKI W., SZOT B., RUSINEK R., BOCIANOWSKI J. 2009. *Estimation of geometric and mechanical properties of seeds of Polish cultivars and lines representing selected species of pulse crops*. Int. Agrophysics, 23: 257–267.
- SADOWSKA U., ŻABIŃSKI A. 2009. *Selected physical properties for seeds of gymnosperm barley grown in a mixture with edible lentil*. Inżynieria Rolnicza, 6(115): 229–236.
- SADOWSKA U., ŻABIŃSKI A. 2011. *Influence of mixed sowing of yellow lupine with gymnosperm barley on the selected physical properties of seeds*. Inżynieria Rolnicza, 6(131): 187–195.
- SEGIT Z., SZWED G., SZWED-URBAŚ K. 2003. *Damage to durum wheat grains as a result of dynamic loading*. Acta Agrophysica, 2(4): 841–849.
- SOLOGUBIK C.A., CAMPAÑONE L.A., PAGANO A.M., GELY M.C. 2013. *Effect of moisture content on some physical properties of barley*. Industrial Crops and Products, 43: 762–767.
- Szczegółowa uprawa roślin. 2003a. Red. Z. Jasińska i A. Kotecki. T. I. Wyd. Akademii Rolniczej, Wrocław.
- Szczegółowa uprawa roślin. 2003b. Red. Z. Jasińska i A. Kotecki. T. II. Wyd. Akademii Rolniczej, Wrocław.
- YALÇIN İ., ÖZARSLAN C., AKBAŞ T. 2007. *Physical properties of pea (Pisum sativum) seed*. Journal of Food Engineering, 79: 731–735.
- ZDYBEL A., GAWŁOWSKI S., LASKOWSKI J. 2009. *Influence of moisture content on some physical properties of rye grains*. Acta Agrophysica, 14(1): 243–255.

**LIMITATION OF CAUCHY FUNCTION METHOD
IN ANALYSIS FOR DOUBLE ESTIMATORS OF FREE
TRANSVERSAL VIBRATION OF CANTILEVER
TAPERED SHAFTS**

Jerzy Jaroszewicz^{1*}, *Łukasz Dragun*²

¹ Faculty of Management

² Faculty of Mechanical Engineering
Białystok University of Technology

Received 5 December 2012; Accepted 6 June 2013; Available on line 15 July 2013

Key words: cantilever shafts, transversal, vibrations, Cauchy function, boundary value problem.

Abstract

In this paper the Bernstein-Kieropian simplest Dunkerly estimators of natural frequencies of cantilever shafts with power variable flexural rigidity and attached concentrated mass were analyzed in a theoretical approach. The approximate solution of boundary value problem of transversal vibrations by means of Cauchy function and characteristic series method has gave getting functional dependence between natural frequency and variable parameters of shafts. Particular attention has been given to a singularity arising from the uncertainty of estimates of Bernstein-Kieropian. Limitation of Cauchy function method in analysis double estimators of natural frequencies of transversal vibration of cantilever tapered shafts exude to exact theoretical selection using by Bessel's function and experimental result received by Panuszka R., Uhl T.

Introduction

In process of designing many structures and structural components such as chimneys towers, head frames, masts, airplane wings and turbine blades it is important to emphasize that they can be modeled by means of a tapered cantilever beam of varying cross section – which works in extremely dynamic loads – we have to know dynamics characteristic like as values and forms of natural vibrations which are necessary to analysis of resonance effect until

* Correspondence: Jerzy Jaroszewicz, Białystok University of Technology, Ojca Tarasiuka street 2, 16-001 Kleosin, e-mail: j.jaroszewicz@pb.edu.pl

starting and braking. These elements can be modeled by cantilever beams with variable parameters in which they are more importantly distributed: rigidity, mass, module, resilience, cross section, rigidity of bearing, axial loads. Sometimes it is necessary to consider discrete inclusions in distributed masses and form base rigidity. In general terms the solution to those problems is difficult but possible to solve as listed in a few cases below.

In papers (LAN, SUPPINGER, TALEB 1945) have solved boundary value problem of cantilever tapered beam by Bessel's function. Existing equation of transversal vibrations power variable of cross – these section might have variable Euler's form and then general integral is formulating by elementary function (LAN, PANUSZKA, UHL 1983).

More often studies beams like these are applying analytical and first of all numerical approximate methods. Applying these in theory it is difficult estimate accuracy calculated characteristics without knowing exact value for chosen special case.

Between numerical methods widely applying have finite elements methods and finite difference method (JAROSZEWICZ, ZORYJ 2000) and transfer matrix method which J. Jaroszewicz has applied earlier in his paper. The example of analytical approach is variation method – although it does not warrant high accuracy that include particular form of vibration – however, this gives very simple form of solution (GOEL, 1976, TIMOSHENKO, GERE 1963). It's crucial to remember the sequenced approximation. On this base of variable cross – section, which has more complicated form (MIKELADZE 1951). Application of Green's function method in frequency analysis of axisymmetric vibration of annular platter with elastic ring supports (KUKLA, SZEWCZYK 2005). The method of partial discretization in free vibration problems of circular plates with variable distribution of parameters (JAROSZEWICZ et al. 2006, JAROSZEWICZ, ZORYJ 2006). Furthermore free vibrations of a system of non-uniform beams coupled by elastic layers has been considered (KUKLA, ZAMOJSKA 2006). Free vibrations of axially loaded stepped beams has been analysed by using a Green's function method (KUKLA, ZAMOJSKA 2007).

Disregarding papers that considerate simultaneously few variable parameters, we move on to articles that deserves our attention, like work of L.M. Zoryj and J. Jaroszewicz that is applying influence function method and characteristic series to solving those problem. This proposition was developed in common works (JAROSZEWICZ, ZORYJ 1987, 2000). Spectral function method which were proposed by Bernstein was applied to analysis constant parameters system, without consideration friction (BERNSTEIN, KIEROPIAN 1960). L.M. Zoryj and J. Jaroszewicz have improved his method to boundary value problems of transversal and torsion vibrations of beam and shafts in there papers published in JAROSZEWICZ, ZORYJ (1994).

They received general formulas other scribed the coefficient of characteristic series for variable form of cantilever beam.

In paper (JAROSZEWICZ, ZORYJ 1990) have obtained formulas which can be applied to engineering practice for calculation fundamental natural frequency transversal vibrations non-homogeneous beams and shafts, and have formulated conditions of those applying.

In this paper the boundary value problem of cantilever with variable distributed flexural rigidity and mass along the cantilever axis, (M – concentrated mass, l – length of beam, x, y – coordinates) was presented. The result is general form characteristic equation allowing design estimates of the vibration and estimates of critical power (AUCIELLO 2001, JAROSZEWICZ, ZORYJ 1999).

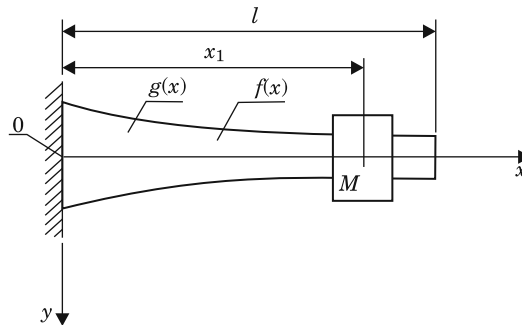


Fig. 1. Substituted model of cantilever of variable cross – section
Source: JAROSZEWICZ, ZORYJ (1997).

Presented substituted model is corresponding assembly shafts with tapered shaft neck which were applied in machines like grinding machines, radial fans and pumps (JAROSZEWICZ, DRAGUN 1994).

In classic exist to formulate boundary value problem of transversal vibration presented in figure 1 is necessary to considerate except conditions on ends ($x = 0, x = l$) fourth conditions in place of attached mass $\mu(x = x_1)$. In this method mass inclusion is considerate in exist equation by Dirac's function (GOEL, 1976, JAROSZEWICZ, ZORYJ 1997).

The proposed method allows more to solve problem.

Definition of the problem

Transversal free vibrations of the model of a cantilever of figure 1 are governed by the equation:

$$L[y] - \alpha_1 f(x_1) \delta(x - x_1) y(x_1) = 0 \quad (1)$$

where $L[y]$ denotes the differential operator

$$L[y] = y^{IV} + \frac{2f'(x)}{f(x)} y''' + \frac{f''(x)}{f(x)} y'' - \omega^2 v(x) y \quad (2)$$

and

$$f(x) = EI(x), \alpha_1 = f(x), \alpha_1 = \omega^2 M, (x) = \frac{g(x)}{f(x)} \mu = \frac{M}{m_0 l} \quad (3)$$

δ is the Dirac function and prime denotes derivative with respect to x , ω – parameter of frequency. The boundary conditions are

$$y(0) = y'(0) = 0, y''(l) = y'''(l) = 0 \quad (4)$$

The characteristic equation

The general solution to the equation (2) has the following form GOEL (1976), JAROSZEWICZ, ZORYJ (1997):

$$y(x, \alpha) = C_0 Q(x, \alpha) + C_1 \dot{Q}(x, \alpha) + C_2 \ddot{Q}(x, \alpha) + C_3 \dddot{Q}(x, \alpha) \quad (5)$$

where

$$Q(x, \alpha) = K(x, \alpha) + \alpha f(x_1) K(x_1, \alpha) K(x, x_1) \quad (6)$$

and C_0, C_1, C_2, C_3 are arbitrary constants, $K(x, \alpha)$ is the Cauchy function of the equation $L[y] = 0$, $\Phi(x, \alpha) = K(x, \alpha) \Theta(x - \alpha)$ is the influence function, $\Theta(x)$ denotes the Heaviside function α is a parameter, and dot denotes derivative with respect to the parameter α .

The result substituted of expressions (5) boundary conditions (4) received characteristic equation:

$$\Delta \equiv [K''(x, \alpha) K'''(x, \alpha) K''''(x, \alpha) K(x, \alpha)] + \alpha_1 f(x_1) [K''''(x, \alpha) K''(x, x_1) K(x_1, \alpha) + K''(x, \alpha) K''''(x, x_1) K(x_1, \alpha)] = 0 \quad \left. \begin{array}{l} x=l \\ \alpha=0 \end{array} \right\} \quad (7)$$

where accepted designation:

$K(x_1, \alpha) = K_1 \alpha K(x, x_1) = K_{x_1}$ and $\alpha = 0$, what is possible, when rigidity $f(x)$ has positive value. Most often in practice concentrated mass meet attachment case of the free end of support $x = l$, from which equation has the form:

$$\Delta \equiv F_{01} - r_1 F_4' = 0 \quad \left| \begin{array}{l} x = x_1 l \\ \alpha = 0 \end{array} \right. \quad (8)$$

where

$$F_{01} = K''_{x\alpha} K''_{x\alpha} - K''_{x\alpha} K''_{x\alpha} \quad (9)$$

$$F_4' = K''_{x\alpha} K_{x\alpha} - K''_{x\alpha} K_{x\alpha}$$

Functions (9) and it combination have practical application (JAROSZEWICZ, ZORYJ 1997).

In equation (8) considered, that $K''(l,l)$ and $K'''(l,l) = 1$, which results from Cauchy's function.

$$F_4' = 0 \quad \left| \begin{array}{l} x = x_1 l \\ \alpha = 0 \end{array} \right. \quad (10)$$

This corresponds articulated supported position the right end of the beam. In the general case Cauchy's function can be create in power series relative variable x or relative square of the frequency parameter ω^2 .

In this case the second method is used, what gives the following form of the function $K(x, \alpha)$

$$K(x, \alpha) = \sum_{i=1}^{\infty} (-\omega)^{2i} K_i(x, \alpha) \quad (11)$$

where

$$K_0(x, \alpha) = f(\alpha) \int_{\alpha}^x \frac{(x-s)(s-\alpha)}{f(s)} ds \quad (12)$$

$$K_i(x, \alpha) = \int_{\alpha}^x v(t) K_0(x, t) K_{i-1}(t, \alpha) dt, \quad i = 1, 2, 3 \quad (13)$$

After introduction of signs

$$J_0(x, \alpha) = \int_{\alpha}^x \frac{(x-s)(s-\alpha)}{f(s)} ds \quad (14)$$

$$J_1(x, \alpha) = \int_{\alpha}^x \mu(t) \cdot J_{i-1}(t, \alpha) \cdot dt \quad (15)$$

series (11) can be written as:

$$F_{01} = f^2(\alpha) = \sum_{k=0}^{\infty} (-\omega)^{2k} a_k \quad (16)$$

$$F_4' = f^2(\alpha) = \sum_{k=0}^{\infty} (-\omega)^{2k} b_k \quad (17)$$

$$a_k = \sum_{i=0}^k (J_i'' J_{k-1}'''' - J_i'''' J_{k-1}'') \quad (18)$$

$$b_k = \sum_{i=0}^k (J_i J_{k-1}'' - J_i'' J_{k-1}), \quad k = 1, 2, 3 \quad (19)$$

Determination of the basic frequency of a cantilever beam

Trough suitable transformations including expression (11) from the equation (7) we received a characteristic series:

$$\Delta \equiv \sum_{k=0}^{\infty} (-\omega)^{2k} A_k = 0, \quad k = 0, 1, 2, 3, \dots \quad (20)$$

Three coefficients defined by formulas:

$$A_0 = 1 \quad (21)$$

$$A_1 = \int_0^l g(t) \int_0^t \frac{(t-s)^2}{f(s)} ds dt + M \int_0^l \frac{(l-s)^2}{f(s)} ds \quad (22)$$

$$A_2 = \left\{ \int_0^l g(t) \int_0^t \frac{t(s-t)}{f(s)} ds dt \right\} \left\{ \int_0^l g(t) \int_0^t \frac{s(t-s)}{f(s)} ds dt \right\} + M \left\{ - \int_0^l g(t) J_0(l, t) \left[\int_0^t \frac{(t-s)(s-l)}{f(s)} ds \right] dt + \int_0^l g(t)(l-t)[J_0(l, 0)J_0(t, 0) - J_0(l, 0)J_0(t, 0)] dt \right\} \quad (23)$$

With coefficients A_0, A_1, A_2 series (20) can calculate the basic vibration frequency applying Bernstein bilateral estimators (MIKIEŁADZE 1951):

$$\frac{A_0}{\sqrt{A_1^2 - 2A_0A_2}} \leq \alpha \omega_0^2 \leq \frac{2A_0}{A_1 + \sqrt{A_1^2 - 4A_0A_2}} \quad (24)$$

The particular case where concentrated M is much higher than solid beam mass:

$$\int_0^l \rho(x) S(x) dx \ll M \quad (25)$$

The characteristic equation (7) can be represented in the form:

$$1 + r_1 f(x_1)[(x - \alpha) J_0(x, \alpha) - J_0(x, \alpha)] = 0 \quad \left| \begin{array}{l} x = x_1 = l \\ \alpha = 0 \end{array} \right. \quad (26)$$

Received the following formula on square of the frequency appropriate replacement system with one degree of freedom:

$$\alpha \omega_0^2 = \left[M \int \frac{(l-t)}{f(t)} dt \right]^{-1} \quad (27)$$

Simple calculations selected shafts and cantilever beams shaped taper

Stiffness and mass can be described by the formulas:

$$f(x) = El_0 \left(1 - \gamma \frac{x}{l} \right)^n, \quad g(x) = m_0 \left(1 - \gamma \frac{x}{l} \right)^m \quad (28)$$

$$\gamma = \frac{l - H}{l} \quad (29)$$

where

$$I = I_1 + H \quad (30)$$

where

E is the modulus Young's, I_0 , m_0 appropriate moment of inertia and mass per unit length of the beam at base, n , m – parameters of the beam cross – section, which may take the actual ($n = 2m$). Concentrated mass M , attached on the end of beam, included by way of $\mu = \frac{M}{m_0 l}$.

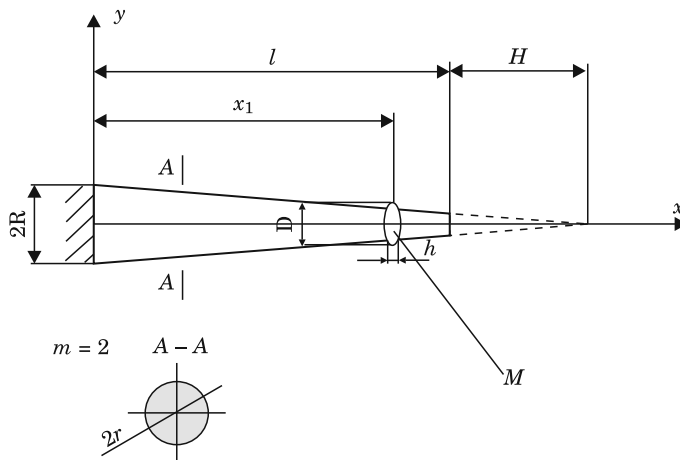


Fig. 2. Beam schematic

Considered stiffness of the beam in figure 2 under the general formula (2, 4, 5) in paper (JAROSZEWICZ, ZORYJ 1999), which found strict expression describing the function Cauchy ($n = 4$) (JAROSZEWICZ, ZORYJ 1985):

$$\phi(x, \alpha) = \frac{(x, \alpha)^3}{6 \cdot EJ_0 \cdot (1 - k \cdot x)^2 \cdot (1 - k \cdot \alpha)^2} \quad (31)$$

where

$$k = \frac{\gamma}{l} \quad (32)$$

As a first example been considered homogenous beam in the form truncated taper in fig. 2, axis x aimed along the axis taper the beginning at the center base with a radius R .

Enter the following markings: H – full height complement of taper, ρ – density of the material, γ – coefficient convergence. Stiffness and mass of taper describe formulas (29), when $n = 2, m = 4, I_0 = \frac{1}{4} \pi R^4, m_0 = \pi \rho R^2$.

Coefficient $\gamma = 0$ corresponds for shafts in the shape of a cylinder.

For shafts in the shape of a cone with a taper $\gamma = 0$ and $\gamma = 1$ at the end of the fixed weight concentrated disc shaped small size. In this assumption: $\frac{D}{l} \leq \frac{1}{6}$ and, $\frac{h}{D} \leq \frac{1}{4}$ since they do not meet at the considered geometry – the moment of inertia of the disk and make the boundary conditions (MARTIN 1956, PANUSZKA, UHL 1983).

The case $\gamma = 1$ and $\mu \neq 0$ is a singular zero due to the stiffness of the cone at its apex full, that is, the mounting mass. Taking into account equations (29), the integrals are calculated in Expressions (22), (23) to give a series of characteristic as follows:

$$1 + \left[\frac{5-4\gamma}{60} + \frac{\mu}{3(1-\gamma)} \right] \alpha \omega^2 + \frac{1}{360} \left[\frac{1}{\gamma^8} + \frac{\varphi_1(\gamma)}{28\gamma^8} + \mu \frac{\varphi_2(\gamma)}{\gamma^7(1-\gamma)} \right] \alpha^2 \omega^4 - \dots = 0 \quad (33)$$

where

$$\varphi_1(\gamma) = 4\gamma^7 + 14\gamma^6 + 84\gamma^5 - 875\gamma^4 + 1820\gamma^3 - 1470\gamma^2 + 420\gamma + 420(I-\gamma)^4 \ln(I-\gamma) \quad (34)$$

$$\varphi_2(\gamma) = \gamma^7 + \gamma^6 + 3\gamma^5 + 15\gamma^4 - 110\gamma^3 + 150\gamma^2 - 60\gamma + 60(I-\gamma)^3 \ln(I-\gamma) \quad (35)$$

$$\alpha = \frac{m_0 l^4}{E J_0} \quad (36)$$

Where γ takes a small value to calculate the function (34) is preferably used instead of the exact patterns corresponding ranks.

$$\frac{\varphi_1(\gamma)}{\gamma^8} = -420 \cdot 24 \left(\frac{3!}{8!} + \frac{4!}{9!} + \frac{5!}{10!} \gamma^2 + \dots \right) \quad (37)$$

$$\frac{\varphi_2(\gamma)}{\gamma^7} = 1 - 360\left(\frac{3!}{8!} + \frac{4!}{9!} + \frac{5!}{10!} \gamma^2 + \dots\right) \quad (38)$$

For the special case when γ tends to 0, the series (33) takes the form:

$$1 + \frac{1}{12} (1 + 1\mu) \alpha \omega^2 + \frac{1}{71} (1 + 8\mu) \alpha^2 \omega^4 + \dots = 0 \quad (39)$$

when for $\mu = 0$ has following form:

$$1 + \left(\frac{5 - 4\gamma}{60}\right) \alpha \omega^2 + \frac{1}{360} \left(\frac{1}{8} + \frac{\varphi_1(\gamma)}{28\gamma^8}\right) \alpha^2 \omega^4 + \dots = 0 \quad (40)$$

The rough estimate described in $\overline{\text{BERSTEIN, KIEROPIAN (1960)}}$ can be obtained from (33) in following form:

$$\alpha \omega_0^2 \approx = \frac{3(1 - \gamma)}{\frac{1}{3} (3 - 3\gamma + \gamma^2) + \mu} \quad (41)$$

The simplest “course estimate of the” lower basic rate determined by the formula Dunkerly’a ($\overline{\text{JAROSZEWICZ et al. 2008}}$):

$$\alpha \omega_0^2 \underline{=} = \frac{60(1 - \gamma)}{(5 - 4\gamma)(1 - \gamma) + 20\mu} \quad (42)$$

To the “rough estimate” above the fundamental frequency, applied mark $\alpha \omega_0^2 \overline{=}$.

$$\alpha \omega_0^2 \overline{=} = \frac{3(1 - \gamma)}{\mu} \quad (43)$$

Accurate estimates of the bottom of the base rate $\alpha \omega_0^2 \underline{=}$ and top $\alpha \omega_0^2 \overline{=}$ was calculated from the formulas Bernstein (24). It should be noted that, with the first three coefficients of characteristic series may also be calculated on the other frequency estimators bilateral their approximate estimates of the third and fourth frequencies.

Discussion of results of double-sided estimators of the basic frequency

On the basis of the frequency equation (8), after solving integrals (23) and for applying estimators (24) calculations results were achieved that are introduced in table 1.

Additionally in approximate estimators were presented from the top and bottom and course estimator from the bottom, based on mathematical formulas (41, 42, 43).

Graphical dependences of appropriate estimators on the coefficient of the gamma similarity without concentrated mass ($\mu = 0$) is presented on figure 3 as well as at different ratio values of the concentrated mass to constant mass they presented on figure 4 and figure 5. From graph in figure 3 we can conclude, that difference between arithmetic means of estimators for the cylinder (that is $\gamma = 0$) amounts to the 2.4% in relation to the direct value 12.36 and for the sharp cone $\gamma = 1$ amounts to the 0.63% towards the direct value 75.73.

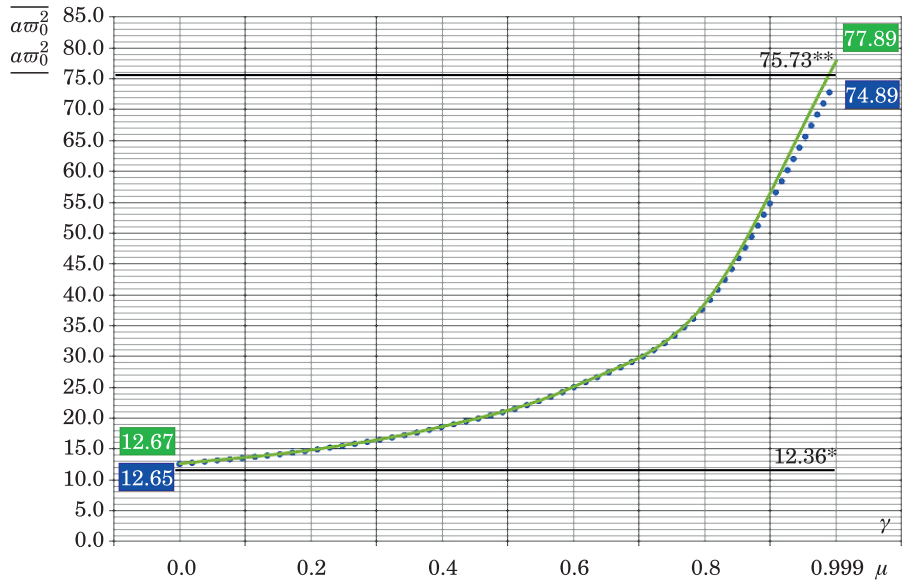
Theoretical calculations confirms experimental results received in Panuszka R. papers, Uhl T and with direct theoretical results – sharp cone 75.75. ($\gamma = 1$, and $\mu = 0$) and for the cylinder ($\gamma = 0$ and $\mu = 0$) received by Tymoshenko S.P., quoted in positions (GOGEL 1976, KUKLA, SZEWCZYK 2005). In considered shaft cases even comparatively small concentrated mass that is put on their endings (figure 4 and figure 5) lowering a great deal of the basic frequency. The rate of the γ similarity causes the increase in the frequency for beams without mass or with very small mass ($\mu \leq 0.001$) what results from graphs on figure 4. Course estimators from above and from the bottom (figure 5), are calculated on the basis of very simple formula from the table 2.3 (JAROSZEWICZ, ZORYJ 1997) and the bottom estimators are calculated on the basis of formula (42) deduced from the Dunkerly's formula (BERNSTEIN, KIEROPIAN 1960) that are giving good calculation accuracy (up to the 5%) for many practical cases which are meeting the conditions from the table 2.4 (JAROSZEWICZ, ZORYJ 1997). Patterns from the table 2.3 (JAROSZEWICZ, ZORYJ 1997) are giving a good approximation at $\mu \geq 5$, formula (42) is giving a close approximation to the accurate value at any given values μ . Pattern (41) can be applied, when $\gamma > 0$ and $\mu < 5$. Graph figure 5. is illustrating this process.

From graphs in figure 5 one can see, that estimators of the basic frequency at $\gamma \rightarrow 1$ are making their way to 0. At grate enough value μ ($\mu \geq 5$) curves $\mu \alpha \omega_0^2$ (solid lines) from figure 5 are identical with appropriate curves $\mu \alpha \omega_0^2$ from figure 4, how it should be.

Table 1

Results of calculation of estimators: accurate ($\alpha_{\omega_0^2}$, $\alpha_{\omega_0^2}$), approximate ($\alpha_{\omega_0^2}$, $\alpha_{\omega_0^2}$), rough ($\alpha_{\omega_0^2}$)

V	μ	A_0	A_1	A_2	$\alpha_{\omega_0^2}$	$\alpha_{\omega_0^2}$	$\alpha_{\omega_0^2}$	$\alpha_{\omega_0^2}$	$\alpha_{\omega_0^2}$	$\alpha_{\omega_0^2}$	$\alpha_{\omega_0^2}$	$\mu\alpha_{\omega_0^2}$	$\mu\alpha_{\omega_0^2}$	$\alpha_{\omega_0^2}$
0	1	1	0.416667	0.000347	2.404814	2.404819	1.500000	3.000000	2.400000	2.404814	2.404819	3.000000	2.404819	2.400000
0.2	1	1	0.480667	0.002104	2.073828	2.073917	1.323529	2.400000	2.054795	2.073828	2.073917	2.400000	2.073917	2.054795
0.4	1	1	0.612222	0.002479	1.644306	1.644343	1.088710	1.800000	1.633394	1.644306	1.644343	1.800000	1.644343	1.633394
0.6	1	1	0.876667	0.002949	1.145086	1.145095	0.789474	1.200000	1.140684	1.145086	1.145095	1.200000	1.145095	1.140684
0.8	1	1	1.696667	0.003753	0.590161	0.590161	0.424528	0.600000	0.389391	0.590161	0.590161	0.600000	0.590161	0.589391
0.99	1	1	33.350667	0.005665	0.029985	0.029985	0.022443	0.030000	0.029984	0.029985	0.029985	0.030000	0.029985	0.029984
0	2.5	1	0.916667	0.000347	1.091360	1.091360	0.857143	1.200000	1.090909	2.728400	2.728401	3.000000	2.728401	2.727273
0.2	2.5	1	1.111667	0.004888	0.903130	0.903137	0.724346	0.960000	0.899550	2.257825	2.257843	2.400000	2.257843	2.248876
0.4	2.5	1	1.445556	0.005677	0.693663	0.693665	0.570825	0.720000	0.691776	1.734157	1.734163	1.800000	1.734163	1.729439
0.6	2.5	1	2.126667	0.006850	0.470933	0.470934	0.397351	0.480000	0.470219	1.177333	1.177335	1.200000	1.177335	1.175549
0.8	2.5	1	4.196667	0.008856	0.238404	0.238404	0.205950	0.240000	0.238284	0.596011	0.596011	0.600000	0.596011	0.595711
0.99	2.5	1	83.350667	0.013391	0.011998	0.011998	0.010576	0.012000	0.011998	0.029994	0.029994	0.030000	0.029994	0.029994
0	5	1	1.750000	0.000347	0.571493	0.571493	0.500000	0.600000	0.371429	2.857467	2.857467	3.000000	2.857467	2.857143
0.2	5	1	2.153333	0.009430	0.465344	0.465345	0.412844	0.480000	0.464396	2326718	2326723	2.400000	2326723	2321981
0.4	5	1	2.834444	0.011007	0.35328?	0.353288	0.318396	0.360000	0.352803	1.766436	1.766438	1.800000	1.766438	1.764014
0.6	5	1	4.210000	0.013354	0.237709	0.237709	0.217391	0.240000	0.237530	1.188544	1.188545	1.200000	1.188545	1.187648
0.8	5	1	8.63333	0.017371	0.119599	0.119599	0.110837	0.120000	0.119570	0.397996	0.397996	0.600000	0.397996	0.397848
0.99	5	1	166.68400	0.026684	0.005999	0.005999	0.005621	0.006000	0.005999	0.02999?	0.02999?	0.030000	0.02999?	0.029997
0	0	1	0.083333	0.000347	12.649111	12.668737	3.000000	-	12.000000	0.000000	0.000000	-	0.000000	-
0.2	0	1	0.070000	0.000184	14.853411	14.865645	2.950820	-	14.285714	0.000000	0.000000	-	0.000000	-
0.4	0	1	0.056667	0.000165	18.631297	18.662092	2.755102	-	17.647059	0.000000	0.000000	-	0.000000	-
0.6	0	1	0.043333	0.000141	25.028880	25.127497	2307692	-	23.076923	0.000000	0.000000	-	0.000000	-
0.8	0	1	0.030000	0.000106	38.137621	38.613054	1.451613	-	33.333333	0.000000	0.000000	-	0.000000	-
0.999	0	1	0.016733	0.000050	74.534271	77.887461	0.008991	-	59.760956	0.000000	0.000000	-	0.000000	-



* for the support of the fixed section, ** for the taper support sharp
 Fig. 3. Independence graph of the accurate frequency estimates obtained for $\mu = 0$, based on the formula (4, 5) Values accurate by (KRISHMA MURTY, PRABAHAKARAN 1969)

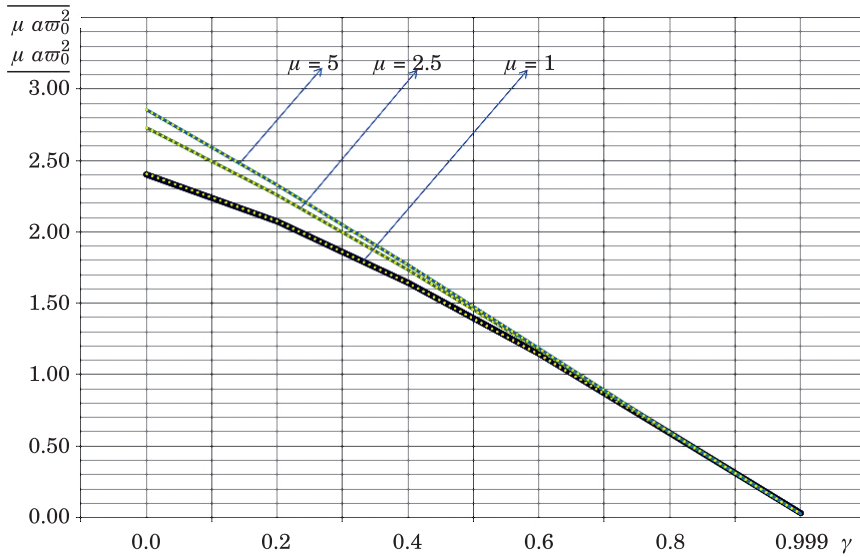


Fig. 4. Independence graph of multiplications accurate estimators through concentrated weight ratio for continuous

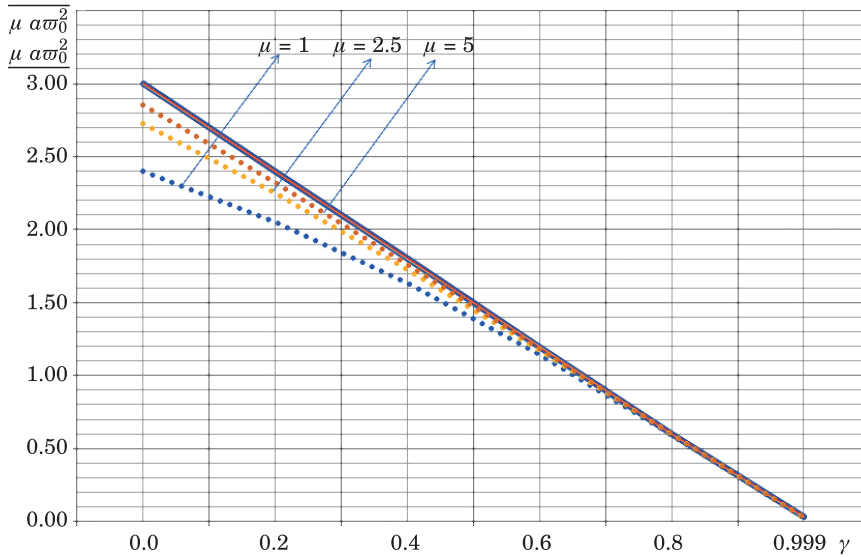


Fig. 5. Independence graph of multiplications approximate estimators through concentrated weight ratio for continuous

Summary

In presented papers there is an analysis of applied derive formulas restrictions by Zoryj and of Jaroszewicz in theirs earlier papers. For example cone shaped crankshaft about the convergence from $\gamma = 0$ to $\gamma = 1$ with mass fastened at the end and concentrated in small disk shape. Establishing that: $D/l \leq 1/6$ and $h/D \leq 1/4$ (fig. 2).

At sharp taper without mass at the end one should apply accurate estimators and applying coarse estimators is inadmissible. In case of mass concentrated truncated cones it is possible to apply approximate estimators and coarse estimators at mass ratio above 5, because their values become levelled. The theory corresponds to the physics description of oscillation because the sharp cone at the end has a zero stiffness and even the smallest concentrated mass can't be fixed on it.

It is showed that it is possible to get a high accuracy of calculations – bring closer bottom and upper estimators and taking into account two first row rates of the characteristic A_1 and A_2 , which significantly simplifies calculations and takes into account a stiffness of the crankshaft and a discrete mass interjection.

The accepted model includes the rotors class on bungs of which undersized shields are planted. In the future it seems too by intentional to expand this

method to outsize rotors planted on conical bungs in it with taking into account of the Timoshenko effect, of i.e. stresses cutting and of the inertia of the rotation of the diameter.

A high accuracy of calculations confirms base frequency calculation error to 0.63% for the sharp cone in relation to rigorous solution received from Bessela function.

Translated by AUTHORS

References

- AUCIELLO N.M. 2001. *On the transverse vibrations of non – uniform beams with axial loads and elastically restrained ends*, International Journal of mechanical Sciences, 43: 193–208.
- BERNSTEIN S.A., KIEROPIAN K.K. 1960. *Opređenje nastot kolebanij strzneych system metodomspektralnoi funkcji*. Gosstroizdat, Moskva.
- CEM ECE M., AYDOĞDU M., TASKIN V. 2007. *Vibration of a variable cross – section beam*. Mechanics Research Communications, 34: 78–84.
- DOMORADZKI M., JAROSZEWICZ J., ZORYJ L. 2005. *Analysis of influence of elasticity constants and material density on base frequency of axi-symmetrical vibrations with variable thickness plates*. Journal of Theoretical and Applied Mechanics, 43(4): 763–775.
- GOEL R.P. 1976. *Transverse vibrations of tapered beams*. Journal of Sound and Vibration, 47: 1–7.
- JAROSZEWICZ J., DRAGUN Ł. 2012. *Metody diagnostyki wibroakustycznej młynów węglowych wentylatorowych w Elektrociepłowni Białystok S.A.*, Energia w Nauce i Technice, Białystok – Kleosin, p. 43–54.
- JAROSZEWICZ J., MISIUKIEWICZ M., PUCHALSKI W. 2008. *Limitations in application of basic frequency simplest lower estimators in investigations of natural vibrations circular plates with variable thickness and clamped edges*. Journal of Theoretical and Applied Mechanics, 46(1): 109–121.
- JAROSZEWICZ J., ZORYJ L.M., KATUNIN A. 2006. *Influence of Additional Mass' Rings on Frequencies Axi-Symmetrical Vibrations of Linear Variable Thickness Clamped Circular Plates*. Journal of Theoretical and Applied Mechanics, 44(4): 867–880.
- JAROSZEWICZ J., ZORYJ L. 1985. *Drgania giętnie belki wspornikowej o zmiennym przekroju*. Rozprawy Inżynierskie, 33(4): 537–547.
- JAROSZEWICZ J., ZORYJ L. 1999. *The Effect of Non-homogenous Material Properties on Transversal Vibrations of Elastic Cantilevers*. Prikladnaja Mechanika.- Kijev, 35(6): 103–110.
- JAROSZEWICZ J., ZORYJ L. 2000. *Investigation of the Effect of Axial Loads on the Transverse Vibrations of a Vertical Cantilever with Variable Parameters*, International Applied Mechanics, 36(9): 1242–1251.
- JAROSZEWICZ J., ZORYJ L.M. 1987. *Wpływ parametrów zmiennego przekroju na drgania giętnie belek i wałów wspornikowych*. Rozprawy Inżynierskie, 35(3): 523–534.
- JAROSZEWICZ J., ZORYJ L.M. 2006. *The method of partial discretization in free vibration problems of circular plates with variable distribution of parameters*. International Applied Mechanics, 42(3): 364–373.
- JAROSZEWICZ J., ZORYJ L. 1997. *Metody analizy drgań i stateczności kontynualno-dyskretnych układów mechanicznych*. Rozprawy Naukowe Politechniki Białostockiej, 54: 126.
- KRISHNA MURTY A.V., PRABAHAKARAN K.R. 1969. *Vibration of Tapered Cantilever Beams and Shafts*. Aeronautical Quarterly, 20: 171–177.
- KUKLA S., SZWCZYK M. 2005. *Application of Green's function method in frequency analysis of axisymmetric vibration of annular platter with elastic ring supports*. Scientific Research of the Institute of Mathematics and Computer Science, 1(4): 79–86.
- KUKLA S., ZAMOJSKA I. 2006. *Free vibrations of a system of non-uniform beams coupled by elastic layers*. Scientific Research of the Institute of Mathematics and Computer Science, 1(5): 55–62.
- KUKLA S., ZAMOJSKA I. 2007. *Free vibrations of axially loaded stepped beams by using a Green's function method*. Journal of Sound and Vibration, 300(3–5): 1034–1041.

- LAU J.H. 1984. *Vibration frequencies of tapered bars with end mass*. Journal of Applied Mechanics, 51: 179–181.
- MARTIN A.I. 1956. *Some integrals relating to the vibration of a cantilever beam and approximation for the effect of taper on overtone frequencies*. Aeronautical Quarterly, VII: 109.
- MIKELADZE S.E. 1951. *Novyje metody integrirowanija differencjalnych ura- vnenij i ich prilozenija k zadacam teorii uprugosti*. Moskva, Gostechizdat.
- PANUSZKA R., UHL T. 1983. *Wyznaczenie częstości rezonansowych ciągłych układów mechanicznych na przykładzie belki i płyty drgającej*. Archiwum Budowy Maszyn, XXX, (1–2): 111–123.
- SUPPINGER E.W., TALEB N.J. 1956. *Free Lateral Vibrations of Beam of Variable Cross-section*. ZAMP, 3: 6.
- TIMOSHENKO S.P., GERE J.M. 1963. *Teoria stateczności sprężystej*. Wydawnictwo Arkady, Warszawa.
- JAROSHEVICH E., ZORYJ L.M. 1994. *Izhibnye kolebanija i dinamicheskaja ustojchivost' balok s peremennymi parametrami*. Prikladnaja Mehanika, Kiev, 30(9): 75–81.

IMPACT OF OPTIMIZATION OF ALS POINT CLOUD ON CLASSIFICATION

Wioleta Błaszczak-Bąk^{1,2}, Anna Sobieraj²

¹ Institute of Geodesy
University of Warmia and Mazury in Olsztyn
² Chair of Geodesy
Gdansk University of Technology

Received 5 December 2012; Accepted 6 June 2013; Available on line 15 July 2013.

Key word: optimization, classification, intensity.

Abstract

Airborne laser scanning (ALS) is one of the LIDAR technologies (Light Detection and Ranging). It provides information about the terrain in form of a point cloud. During measurement is acquired: spatial data (object's coordinates X, Y, Z) and collateral data such as intensity of reflected signal. The obtained point cloud is typically applied for generating a digital terrain model (DTM) and a digital surface model (DSM). For DTM and DSM generation it is necessary to apply filtration or classification algorithms. They allow to divide a point cloud into object groups (e.g.: terrain points, vegetation, etc.). In this study classification is conducted with one extra parameter—intensity. The obtained point groups were used for digital spatial model generation.

Classification is a time and work consuming process, therefore there is a need to reduce the time of ALS point cloud processing. Optimization algorithm enables to decrease the number of points in a dataset. In this study the main goal was to test the impact of optimization on the results of a classification. Studies were conducted in two variants. Variant 1 includes classification of the original point cloud where points are divided in the groups: roofs, asphalt road, tree/bushes, grass. On variant 2 before classification, an optimization algorithm was performed in the original point cloud. Obtained from these two variants object groups were used to generate a spatial model, which was then statistically analyzed.

Introduction

Airborne Laser Scanning ALS provides a data in the form of a point cloud. Obtaining such data is possible thanks to integration of a laser scanning system with GPS and INS systems (CSANYI et al. 2005, GREJNER-BRZEZIŃSKA

et al. 2004, TOTH, GREJNER-BRZEZIŃSKA 2004). At this stage, data processing includes filtration or classification. Filtration is a process in which two groups of points are obtained: points representing terrain and non-terrain (BORKOWSKI, JÓZKÓW 2007, BŁASZCZAK-BĄK et al. 2010). Classification is based on point cloud division into object groups. The number of distinguished groups is related to the aim of the classification. Characteristics of each group results from the type of surface from which the laser reflected. Examples are groups like: terrain, vegetation, buildings etc. Point groups representing terrain can be used as a basis for Digital Terrain Model (DTM) generation. Point groups obtained from classification are used for Digital Surface Model (DSM) generation.

Assessment of filtration and classification algorithms can be found in many articles, for example in TÓVÁRI and PFEIFER 2005, the authors presented their proposal to divide algorithms into four group:

- Methods based on morphological filters (e.g.: VOSELMAN, MAAS 2001, ZHANG et al. 2002),
- Methods which use algorithms based on active TIN (Triangulated Irregular Network) modeling, in an iterative way, the algorithm fits a modeling surface with data representing real surface (e.g.: SCHUT 1976, KASS et al. 1988, PFEIFER 1998, ELMQVIS 2002),
- Methods which include point cloud segmentation and aim at usually to three point groups: terrain, buildings and vegetation (e.g.: ROGGERO 2002, TÓVÁRI, PFEIFER 2005, SITHOLE, VOSELMAN 2005).

Detailed analyses of selected filtration and classification algorithms are presented in SITHOLE, VOSELMAN (2004). Existing methods have their limits, which are related to incorrect filtration of points from regions with complex topography. This is the impact for conducting studies in area where filtration and classification algorithms can be developed, modified and tested with various parameters.

Studies on intensity of laser pulse reflection utility were conducted by KATZENBEISSER 2003, SONG et al. 2002, CHARANIYA et al. 2004, WANG and LU (2009), ANTONORAKIS et el. 2008 and others. In Katzenbeisser's studies there is a conclusion that using intensity is difficult and complex. Only for flat surfaces reliable information about a given object can be obtained. Höfle and Pfeifer focus on calibrating intensity.

In this study classification was conducted using intensity as an additional classifying factor. Due to the fact that such way of ALS point cloud processing is time and work consuming, the authors proposed to apply point cloud optimization. Optimization conducted before filtration shorten time necessary for DTM generation about 4–6 times in comparison to standard methodology (BŁASZCZAK-BĄK et al. 2010a, 2010b, 2011a). During optimization points

which are not significant for the DTM generation are removed (BŁASZCZAK 2006). The lack of those points and subsequently intensities related to them, was tested in the scope if it has an impact on the point set used for DTM generation.

Intensity ranges for specific types of objects were based on indicated points representing given object. Studies were conducted in two variants. In variant 1 classification was based on an original point set, while in variant 2 classification was preceded by optimization, which reduced the number of points in the dataset. Resulted object groups and models generated from them were statistically analyzed.

Proposal of ALS data processing scheme

One of the ALS data processing stages is classification. The result of a conducted classification is a group of datasets – points representing various objects. Intensity was a basic parameter for establishing groups of points. Their types and number resulted from analyses of cartographic data and recognition in the field. Of course, there are many methods of classification using the intensity parameter, for example object-based land cover classification (ANTONARAKIS et al. 2008). There also are many software based on specific algorithms (e.g. VRMesh, DTMaster). Method of classification used in this publication is characterized by its simplicity. It enabled to control the process of classification and to conduct analyses on each stage of tests. Authors decided to use such solution, because they did not have access to commercial software for classification.

Distinguished groups in this study are as follows: grass, asphalt road, roofs, trees/bushes and others. The last group includes points that have not been assigned to any previous group. Obtained datasets were a basis for spatial model generation.

The basis for each spatial data model is the choice of basic (spatially defined) geometric elements used to represent objects. Depending on the size of basic geometric element used for spatial model generation, three types of models can be distinguished (IZDEBSKI 2008):

- point models – the basic geometric element is a point,
- linear models – the basic element of the line is made up of a sequence of points,
- surface models – the basic element is the area.

Depending on the location and the shape of basic elements the surface models can be divided into:

- regular models,
- irregular patterns.

In view of the fact that airborne laser scanning provides data in discrete form (as point cloud) it is reasonable that a point model is created. A Digital Spatial Point Model generated from discrete ALS data has the value of the intensity at each point x, y, z located in the model. Digital Terrain Model (DTM) is generated on the basis of two object groups obtained in the classification representing surface of the ground: grass and asphalt road.

The processing of the ALS point cloud was conducted in two versions. In variant 1 classification was taken into account, in variant 2 classification was preceded by the optimization process aimed at reducing the size of the data set. The optimization algorithm, which was used in this study, consists of the following steps (BŁASZCZAK 2006, BŁASZCZAK, KAMIŃSKI 2007, BŁASZCZAK-BĄK et al. 2010):

Step 1: defining test strips in the XY plane, parallel to the Y axis.

Step 2: choice of cartographic generalization method used for reducing the size of the measurement set.

Step 3: using in each profile (in the YZ plane) the chosen method of generalization.

An important step is to select the generalization method in test strips and the selection of appropriate tolerances. Threshold values has a significant impact on the degree of reducing a ALS dataset (the number of points removed). In this study, in the second stage in the optimization algorithm, the method of Visvalingam-Whyatt (V-W) (VISVALINGAM, WHYATT 1992) was used. The generalization procedure using comparative surface V-W has been shown in Figure 1. The implementation of the method V-W is to create the next line which is based on generalized points of triangles (e.g. points 1, 2, 3 form a triangle in the plane YZ with area P_1 , Figure 1b). The calculated area of a triangle is verified with the comparative surface. Its size is defined by the user, depending on the statistical characteristics of a dataset from measurements. If the area of the triangle determined from the measured points exceeds the area of a tolerance triangle, then the second point of analyzed triangle is retained (step 2 in Figure 1b). Subsequently, the triangles are formed further (e.g. a triangle with the area P_2 – Fig. 1c or triangle with area P_3 – Fig. 1d), and their areas are compared with the area of the tolerance triangle. When the area of a tolerance triangle is greater than the area of determined triangle, the second point of formed triangle is removed (e.g. point 4 in Fig. 1d).

For both variants Digital Spatial Point Models (described as DSPMv1 and DSPMv2) and Digital Terrain Models (called DTMv1 and DTMv2, respectively) were generated. DTMs were statistically analyzed. A general scheme of the study is presented in Figure 2.

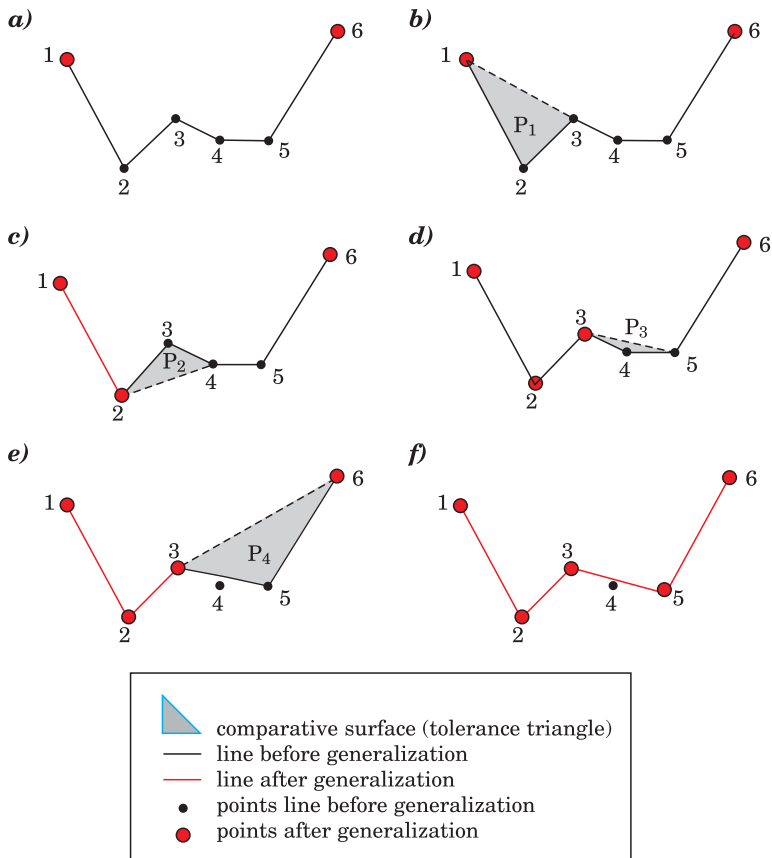


Fig. 1. Stages in line generalization based on comparative surface

Source: VISVALINGAM, WHYATT (1992).

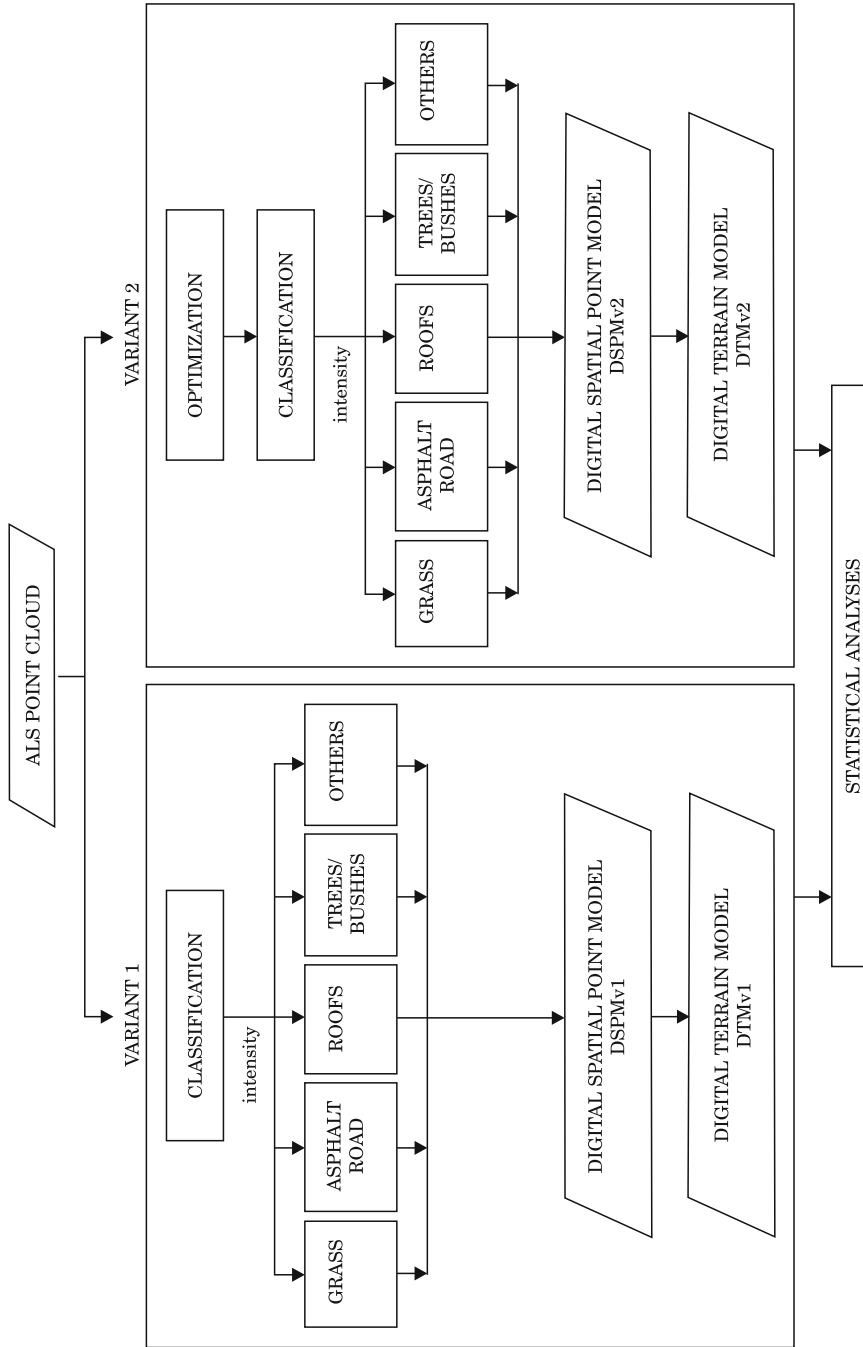


Fig. 2. General scheme of study

Results

The study was based on a point cloud obtained from airborne scanning made by Visimind. For the measurements were used: the Riegl LMS-Q240 laser, Topcon GPS, IMU units and digital cameras. The scan angle was 60 degrees with a resolution of 10,000 Hz. Scanning took place from a helicopter moving at a speed of 50 km/h at an altitude of 700 m. The measured area is located on the outskirts of Olsztyn (Warmia and Mazury). The original data set contained 1.5 million in the format X, Y, Z , intensity. In this study raw data were used for test.

Statistical samples concerning intensity were obtained by identifying and manually selecting the points that belong to the specific object. The results of the analyses are presented in Tables 1–4. The tables use the following code: n – number of points, minimum intensity – I_{\min} , the maximum intensity – I_{\max} , the average value of the intensity – I_{av} , the standard deviation – δ .

Table 1

Intensity for roofs

Object	roof1	roof2	roof3	roof4	roof5	roof6	roof7	roof8	roof9
n	31	9	10	11	22	24	11	13	26
I_{\min}	0.234	0.391	0.425	0.397	0.438	0.430	0.416	0.406	0.385
I_{\max}	0.455	0.458	0.449	0.447	0.460	0.452	0.435	0.448	0.452
I_{av}	0.415	0.432	0.438	0.430	0.447	0.439	0.426	0.429	0.435
δ	0.040	0.021	0.007	0.013	0.006	0.005	0.006	0.014	0.014
Object	roof10	roof11	roof12	roof13	roof14	roof15	roof16	roof17	Roofs
n	20	26	16	18	20	11	15	17	300
I_{\min}	0.378	0.338	0.442	0.399	0.284	0.440	0.446	0.410	0.392
I_{\max}	0.434	0.450	0.455	0.416	0.440	0.461	0.479	0.457	0.450
I_{av}	0.402	0.413	0.449	0.407	0.421	0.452	0.465	0.427	0.431
δ	0.021	0.028	0.004	0.004	0.032	0.006	0.008	0.011	0.014

Table 2

Intensity for asphalt road

Object	asph1	asph2	asph3	asph4	asph5	asph6	asph7	Asphalt road
n	11	20	14	22	16	22	26	131
I_{\min}	0.365	0.349	0.366	0.358	0.341	0.379	0.356	0.359
I_{\max}	0.396	0.392	0.444	0.390	0.394	0.401	0.398	0.402
I_{av}	0.384	0.376	0.392	0.376	0.374	0.392	0.380	0.382
δ	0.009	0.013	0.026	0.009	0.017	0.005	0.012	0.013

Table 3

Intensity for trees/bushes

Object	tree1	tree 2	tree 3	tree 4	tree 5	tree 6	tree 7	tree 8	tree 9	tree 10	Trees/bushes
n	20	26	30	21	29	25	19	29	29	40	268
I_{\min}	0.173	0.100	0.022	0.123	0.245	0.127	0.086	0.353	0.145	0.114	0.149
I_{\max}	0.420	0.411	0.419	0.442	0.434	0.456	0.413	0.417	0.426	0.445	0.428
I_{av}	0.362	0.324	0.305	0.418	0.384	0.365	0.278	0.400	0.359	0.387	0.358
δ	0.064	0.113	0.104	0.067	0.047	0.088	0.114	0.014	0.082	0.063	0.076

Tabela 4

Intensity for grass

Object	Gr1	Gr2	Gr3	Gr4	Gr5	Gr6	Gr7	Gr8	Grass
n	28	14	31	29	24	21	26	23	196
I_{\min}	0.425	0.419	0.417	0.405	0.420	0.413	0.418	0.310	0.403
I_{\max}	0.440	0.444	0.433	0.460	0.435	0.434	0.455	0.454	0.444
I_{av}	0.430	0.433	0.426	0.435	0.428	0.423	0.434	0.430	0.430
δ	0.004	0.007	0.004	0.010	0.005	0.005	0.009	0.028	0.009

Based on the statistical data intensity, ranges for each object group were extracted. The ranges of the intensity are based on the relationship: $\langle I_{\text{av}} - \delta; I_{\text{av}} + \delta \rangle$. Table 5 presents the juxtaposition of intensity ranges for each type of studied object.

Table 5

Intensity ranges for various objects

Objects	Intensity ranges
Roofs	0,417–0,444
Asphalt road	0,369–0,395
Trees/bushes	0,282–0,434
Grass	0,421–0,439

Unfortunately, the result intensity ranges distinguished on the basis of statistical sampling are partially overlapping. In order to clearly define the limits of ranges for each object, ranges were modified. Correct intensity ranges were used to build DSPMs. Analysis also showed that some of the intensity values are not classified to any of the groups, and it is impossible to identify what objects they represent. Not qualified values of intensity (0.00–0.282) and (0.445–0.577) were omitted. Table 6 shows the intensity ranges for each types of objects that have been adopted to build the DSPM.

Table 6

Intensity ranges for DSPM generation

Objects	Intensity ranges
Roofs	0,417–0,420 and 0,440–0,444
Asphalt road	0,369–0,395
Trees/bushes	0,282–0,368 and 0,396–0,416
Grass	0,421–0,493

In a detailed study fragment of the point cloud 83,424 points were used. A processed subset of this ALS point cloud is shown in Figure 3. Given the ALS dataset was processed in two ways. In the first way, only classification was performed. In the secondary, point cloud was optimized and then classified. In both cases, the intensity ranges shown in Table 6 were applied.

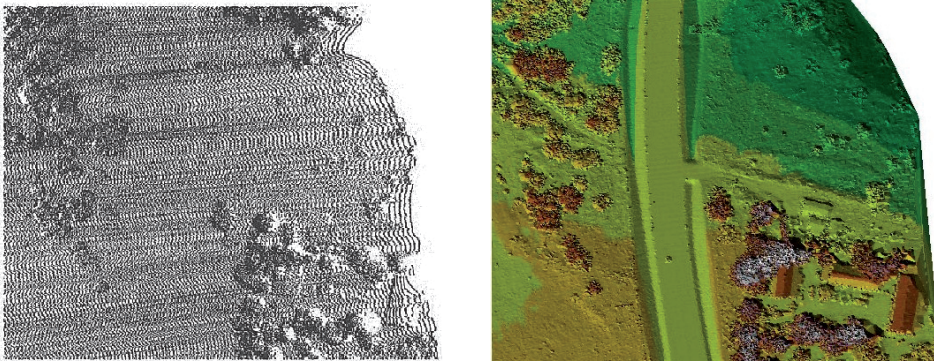


Fig. 3. Fragment of ALS point cloud 83424 points (a), TIN model (b)

Variant 1

ALS point cloud classification was conducted using the previously mentioned ranges of intensity. Obtained results of classification are shown in Figure 4.

The figures indicate that not all the points were correctly classified for the corresponding types of objects. This can be seen especially for the group “roofs’ (Fig. 4b), where beside roof points, there are a lot of points representing trees and bushes. The group “grass’ (Fig. 4a) includes the majority of points. For the group “asphalt road’ (Fig. 4c) the road was classified correctly, but like in the group “roofs’, there also points appear representing trees. As is seen, intensity for the trees has a wide ranges and therefore appeared in all separate groups.

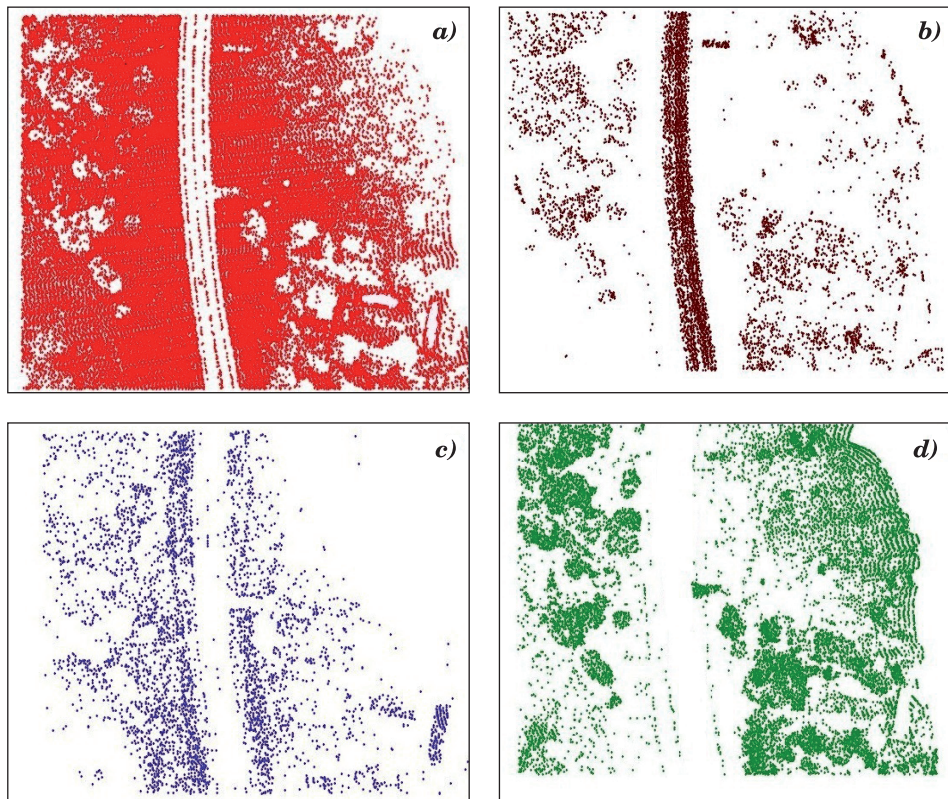


Fig. 4. Variant 1: *a* – grass, *b* – asphalt road, *c* – roofs, *d* – trees/bushes

This resulted from the fact that the measurement was performed when there were leaves on trees. Diversity of leaf color and leaf variable angle relative to the incident laser beam led to the wide range of intensity for trees.

Variant 2

The size of the dataset was reduced using the optimization algorithm. During the reduction, it was assumed that the width of the strip equals 2 m and the area of a tolerance triangle is 0.02 m^2 . This allowed a reduction to 43,715 points.

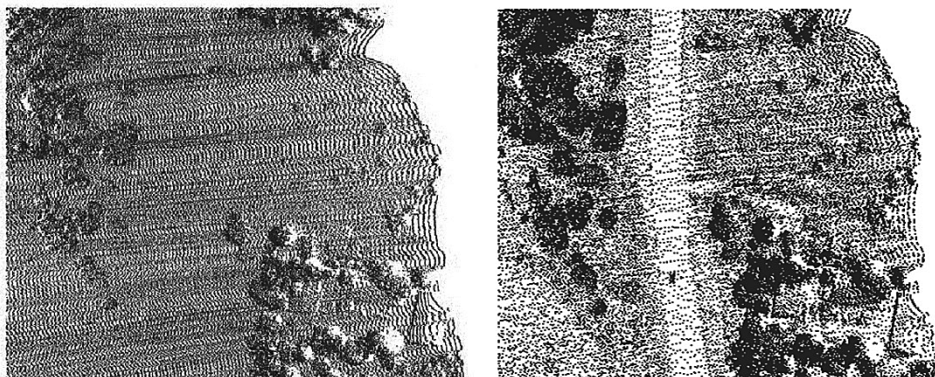


Fig. 5. Original and optimized fragment of ALS point cloud

Optimized dataset were then classified.

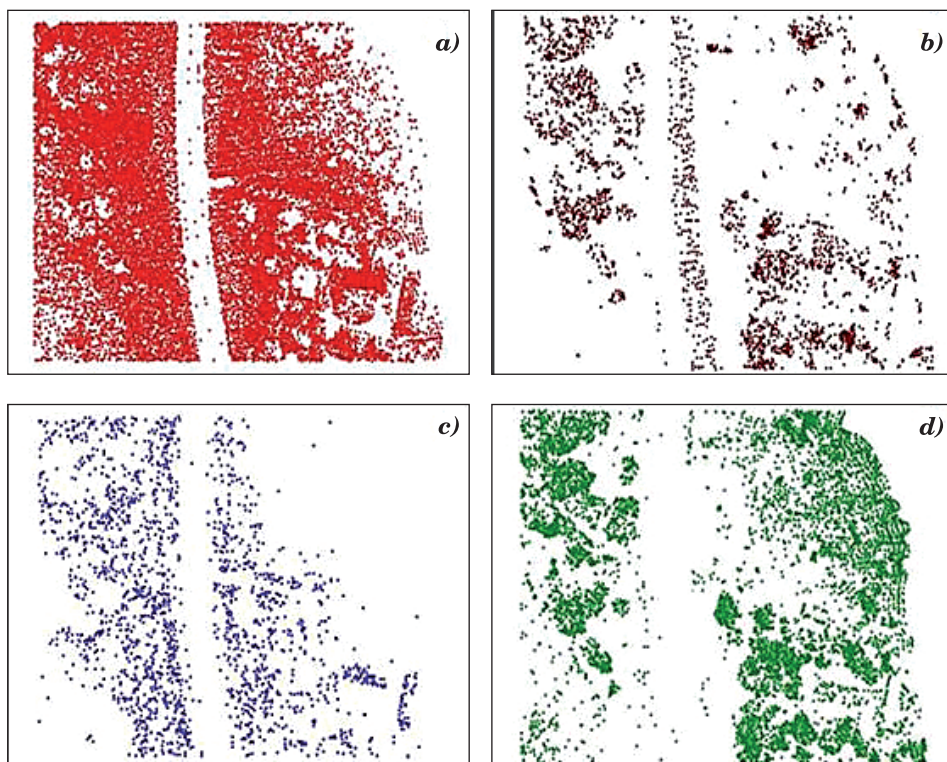


Fig. 6. Variant 2: *a* – grass, *b* – asphalt road, *c* – roofs, *d* – trees/bushes

Figure 6 shows the spatial distribution of the optimized dataset of the point cloud. The effect of optimization can be seen for all groups. The reduction in the number of points is most visible in the groups as asphalt road and roofs. As in Variant 1 classification after the optimization does not give good final results. Manual classification is still needed.

Result analysis

Analyzing the presented results, it is clear that Variant 2, which corresponds to the classification performed on the optimized dataset, allows achieving similar results as in Variant 1. In both cases, asphalt road and grass were well separated. For trees/bushes and the roofs the same mistakes can be observed in both Variants. However, there is no doubt, that a smaller number of points resulting from the optimization process certainly would have an impact on the processing time. Results obtained for the two variants are presented in Table 7.

Table 7

Number of points in groups

Objects	Number of points used for generation	
	DSPMv1	DSPMv2
Roofs	9,891	4,729
Asphalt road	6,102	2,896
Trees/bushes	18,545	10,613
Grass	45,212	20,174
Σ	83,424	43,715
Others	3,674	10,032

Number of points for Digital Models generation in Variant 2 is about 50% less than in Variant 1.

Spatial models generation

Digital Spatial Point Model generation

On the basis of the sets of points from Variant 1 and Variant 2 (Table 7) digital spatial point models were generated. They represent the intensity distribution in the study area. DSPMv1 and DSPMv2 shown in Figure 7.

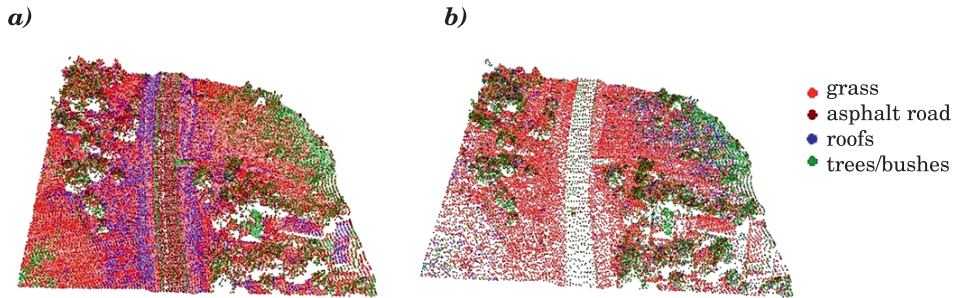


Fig. 7. Digital Spatial Point Models: *a* – DSPMv1, *b* – DSPMv2

Analyzing the two point models, similar point distributions can be observed. The DSPMv2 is more readable due to the reduced number of points. Such models may be useful in the detailed classification, because the observer sees colors that indicates a particular object and also receives information about the height of a point.

Digital Terrain Model generation

Digital Terrain Models were generated from two object groups: grass and asphalt road. Due to the fact that these objects were separated only on the basis of the intensity of the reflection and as previously mentioned, some of these points were misclassified, it was decided to include an additional parameter: the height of the point. Two new subsets of points for Variant 1 and Variant 2 were obtained: a subset of data points showing the terrain generated from the original and then the optimized datasets. Separated subsets became the basis for generating DTMv1 and DTMv2 (Figure 8).

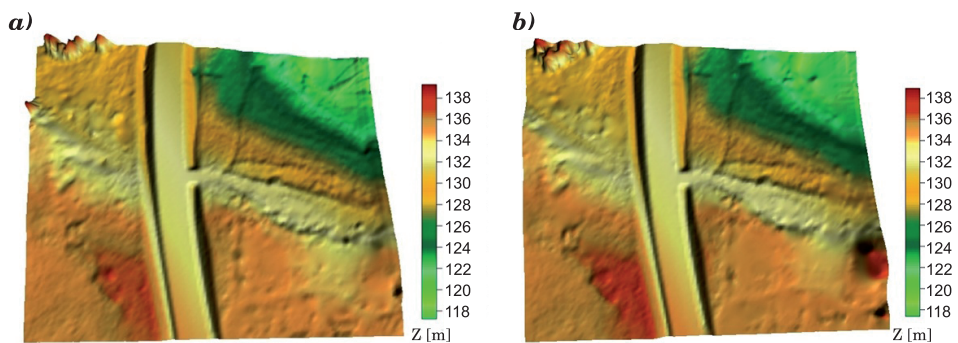


Fig. 8. Digital Terrain Models: *a* – DTMv1, *b* – DTMv2

Additionally, a digital model DTMv3 was generated. It was adopted as the reference model to evaluate the accuracy of obtained two models DTMv1 and DTMv2. DTMv3 was built on the basis of the data obtained after filtration of the original dataset. The most popular method of filtration, the active method TIN model (AXELSSON 2000), was applied here.

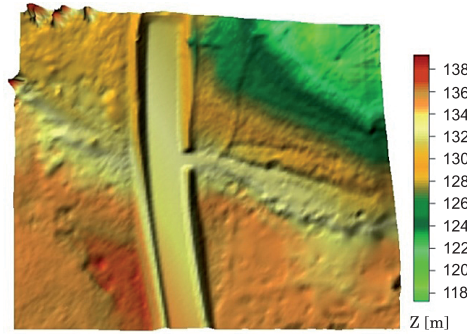


Fig. 9. DTMv3

The three generated DTMs were subjected to statistical comparison. In comparing DTMv1, DTMv2 and DTMv3, the following parameters were applied (OKSANEN, SARJAKOSKI 2005, HEJMANOWSKA et al. 2008):

a) mean error:

$$m_0 = \sqrt{\frac{\sum (z_{\text{mean}} - z_i)^2}{k - 1}} \quad (1)$$

where:

z_{mean} – mean height calculated from two datasets used for DTMs generation,

z_i ($i=1,2., k$) – height of point in data from measurement,

k – number of points in dataset;

b) range $R = z_{\text{max}} - z_{\text{min}}$, where z_{max} – maximum height and z_{min} – minimum height;

c) mean height difference (systematic error):

$$\Delta h_{\text{mean}} = \frac{\sum_{i=1}^k (\tau)}{k} \quad (2)$$

where:

$$\tau = \tau_1 \text{ OR } \tau_2$$

$$\tau_1 = Z_{\text{NMTv}_2} - Z_{\text{NMTv}_1}, \quad \tau_2 = Z_{\text{NMTv}_2} - Z_{\text{NMTv}_1}$$

d) root mean square error (RMSE), describes absolute height accuracy of DTM:

$$\text{RMSE} = \sqrt{\frac{\sum_{i=1}^k (\rho)^2}{k}} \quad (3)$$

where:

$$\begin{aligned} \rho &= \rho_1 \text{ or } \rho_2 \\ \rho_1 &= \tau_1 - \Delta h_{\text{mean}}, \rho_2 = \tau_2 - \Delta h_{\text{mean}}; \end{aligned}$$

e) coefficient of determination (measure of model fitness):

$$D^2 = \frac{\sum_{i=1}^k (Z_{\text{NMTv}_2} - Z_{\text{mean}})^2}{\sum_{i=1}^k (Z_{\text{NMTv}_1} - Z_{\text{mean}})^2} \quad (4)$$

and

$$D^2 = \frac{\sum_{i=1}^k (Z_{\text{NMTv}_2} - Z_{\text{mean}})^2}{\sum_{i=1}^k (Z_{\text{NMTv}_1} - Z_{\text{mean}})^2} \quad (5)$$

A summary of the calculated parameters for assessing the accuracy of the generated DTMs are presented in Table 8.

Table 8

Assessment of DTM

Parameters for assessing the accuracy	DTMv3 reference	DTMv1	DTMv2
m_0	4,655 m	4,675 m	4,662 m
R	21,988 m	21,295 m	21,992 m
Δh_{mean}	-	0,026 m	-0,019 m
RMSE	-	0,299 m	0,168 m
D^2	-	0,991	0,997

The mean error and range for the reference model and the model from Variant 2 have similar values, indicating that the interpolated height of GRID points are comparable. For Variant 1 the mean error is about 2 cm larger, and range is about 70 cm smaller in comparison to the reference model. However, assessment based on such measures does not enable to compare models from

two variants. For such purpose the RMSE and the coefficient of determination were used. Variant 2 achieves better values. RMSE error is about 13 cm lesser, and D^2 is more close to unity. By analyzing obtained values it can be stated that the model generated from the optimized dataset DTMv2 has a better fit for the reference model than the DTMv1.

Conclusions

In this study the results of the classification were presented. The classification criterion was the intensity of the reflected signal. In addition, the optimization process was analyzed as factor changing the size of original datasets. From analyses the following general conclusions can be draw:

- The intensity parameter is not sufficient for the proper distribution of the point cloud to a object group and cannot be the only parameter taken into account in the classification,
- Optimization streamlines the process of classification and generating DSPM and DTM, improves readability of DSPM, does not cause loss of important information.

Specific conclusion can be drawn as follows:

- The intensity assigns for the trees and bushes appears in all selected ranges, in both variants,
- Generated Digital Spatial Models illustrate the point distribution of the intensity parameter for each class of object. Such models may be useful in filtering and classification and in analyzing the propriety of these processes,
- Optimization resulted in a reduction of about 50% of point cloud, but this did not affect the correctness of the classification,
- Digital terrain model generated from an optimized dataset better fits to the reference model which is DTM generated form dataset filtered by means of active TIN model method.

ALS point cloud processing is time and work consuming process, mainly because of the size of dataset. Therefore conducting optimization before such processes is reasonable. Optimization has an impact on efficiency of DTM generated from ALS point cloud.

References

- ANTONORAKIS A.S., RICHARDS K.S., BRASINGTON J. 2008. *Object-based land cover classification using airborne LiDAR*. *Remote Sensing of Environment*, 112: 2988–2998.
- AXELSSON P. 2000. *DEM generation from laser scanner data using adaptive TIN models*. *International Archives of Photogrammetry and Remote Sensing*, XXXIII/4B.
- BLASZCZAK W. 2006 *Optimization of large measurement results sets for building data base of spatial information system*. Doctors thesis. University of Warmia and Mazury in Olsztyn.
- BLASZCZAK-BAK W., JANOWSKI A., KAMIŃSKI W., RAPIŃSKI J. 2010a. *Modification of Lidar Point Cloud Processing Methodology*. FIG Congress. Facing the Challenges – Building the Capacity Sydney, Australia, 11–16 April.
- BLASZCZAK-BAK W., JANOWSKI A., KAMIŃSKI W., RAPIŃSKI J. 2010a. *Modified methodology for analyzing ALS observations*. *Reports on Geodesy*, pp. 7–17.
- BLASZCZAK-BAK W., JANOWSKI A., KAMIŃSKI W., RAPIŃSKI J. 2010b. *Proposition of modification of aerial laser survey point cloud processing methodology*. *Archives of Geomatics “New technology and instruments in survey”*, pp. 7–17.
- BLASZCZAK-BAK W., JANOWSKI A., KAMIŃSKI W., RAPIŃSKI J. 2011a. *Optimization algorithm and filtration using the adaptive TIN model at the stage of initial processing of the ALS point cloud*. *Canadian Journal of Remote Sensing*, 37(6): 583–589.
- BORKOWSKI A., JOŹKÓW G. 2007. *Correctness evaluation of the flakes based filtering method of airborne laser scanning data*. *Archives of Photogrammetry, Cartography and Remote Sensing*, 17a.
- CHARANIYA A., MANDUCHI R., LODHA S. 2004. *Supervised parametric classification of aerial lidar data*. *Proceedings of the Conference on Computer Vision and Pattern Recognition Workshop (CVPRW'04)*, 3: 30.
- CSANYI N., TOTH C., GREJNER-BRZEZINSKA D., RAY J. 2005. *Improving LiDAR Data Accuracy Using LiDAR Specific Ground Targets*. ASPRS Annual Conference, Baltimore, MD, March 7–11, CD-ROM.
- ELMQVIST M. 2002. *Ground surface estimation from airborne laser scanner data using active shape models*. ISPRS, Commission III, Symposium Photogrammetric Computer Vision, September 9–13, Graz, pp. 114–118.
- GREJNER-BRZEZINSKA D., TOTH C., PASKA E. 2004 *Airborne remote sensing supporting traffic flow estimates*. *Proc. of 3rd International Symposium on Mobile Mapping Technology*, Kunming, C 29–31, CD-ROM.
- HANSEN W., VÖGTLE T. 1999. *Extraktion der Geländeoberfläche aus flugzeuggetragenen Laserscanner-Aufnahmen*. *Photogrammetrie Fernerkundung Geoinformation*, pp. 229–236.
- HEJMANOWSKA B., DRZEWIĘCKI W., KULESZA Ł. 2008. *The quality of Digital Terrain Models*. *Archives of Photogrammetry and Remote Sensing*, 18: 163–175.
- IZDEBSKI W. 2008. *Wykłady z przedmiotu SIT/ MAPA zasadnicza*. Politechnika Warszawska.
- KASS M., WITKIN A., TERZOPOULOS D. 1988, *Snakes: Active contour models*. *International Journal of Computer Vision*, 1(4): 321–331.
- KATZENBEISSER R. 2003. *Toposys gmbh technical note*, on line: <http://www.toposys.de/pdfext/>.
- KRAUS K., PFEIFER N. 1998. *Determination of terrain models in wooded areas with airborne laser scanner*. *ISPRS Journal of Photogrammetry and Remote Sensing*, 53: 193–203.
- OKSANEN J., SARJAKOSKI T. 2005. *Error propagation of DEM-based surface derivatives*. *Computers and Geosciences*, 31: 1015–1027.
- ROGGERO M. 2002. *Object segmentation with region growing and principal component analysis*. *International Archives of Photogrammetry and Remote Sensing*, XXXIV/3A.
- SCHUT G.H. 1976. *Review of interpolation methods for digital terrain models*. XIIth Congress of the International Society for Photogrammetry, Helsinki.
- SITHOLE G., VOSSSELMAN G. 2004. *Experimental comparison of filter algorithms for bare-Earth extraction from airborne laser scanning point clouds*. *ISPRS Journal of Photogrammetry and Remote Sensing*, 59(1–2): 85–101.
- SITHOLE G., VOSSSELMAN G. 2005. *Filtering of airborne laser scanner data based on segmented point clouds*. *Geo-Information Science*, 66–71.
- SONG J., HAN S., KIM Y. 2002. *Assessing the possibility of land-cover classification using lidar intensity data*. *International Archives of Photogrammetry and Remote Sensing*, Graz, XXXIV/3B: 259–262.

- TOTH C., GREJNER-BRZEZINSKA D. 2004. *Vehicle classification from LiDAR data to support traffic flow estimates*. Proc. of 3rd International Symposium on Mobile Mapping Technology, Kunming, C 29–31, CD-ROM.
- TOVARI D., PFEIFER N. 2005. *Segmentation based robust interpolation-a new approach to laser data filtering*. IAPRSSIS, 363W19: 79–84.
- VISVALINGAM M., WHYATT J.D. 1992. *Line generalization by repeated elimination of point*. Cartographic Information Systems Research Group, University of Hull.
- VOSSELMAN G., MAAS H.G. 2001. *Adjustment and filtering of raw laser altimetry data*. Workshop on Airborne Laserscanning and Interferometric SAR.
- WANG C., LU Y. 2009. *Potential of ILRIS3D intensity data for planar surfaces segmentation*. Sensors, 9: 5770–5782.
- ZHANG K., CHEN S., WHITMANN D., SHYU M., YAN J., ZHANG C. 2002. *A progressive morphological filter for removing non-ground measurements from airborne LIDAR data*. Journal of Latex Class Files, 1(8).